Estuarine, Coastal and Shelf Science 131 (2013) 245–263

Contents lists available at SciVerse ScienceDirect

Estuarine, Coastal and Shelf Science

journal homepage: www.elsevier.com/locate/ecss

Sediment flux modeling: Simulating nitrogen, phosphorus, and silica cycles

Jeremy M. Testa [a,*], Damian C. Brady [b], Dominic M. Di Toro [c], Walter R. Boynton [d], Jeffrey C. Cornwell [a], W. Michael Kemp [a]

[a] Horn Point Laboratory, University of Maryland Center for Environmental Science, 2020 Horns Point Rd., Cambridge, MD 21613, USA
[b] School of Marine Sciences, University of Maine, 193 Clark Cove Road, Walpole, ME 04573, USA
[c] Department of Civil and Environmental Engineering, University of Delaware, 356 DuPont Hall, Newark, DE 19716, USA
[d] Chesapeake Biological Laboratory, University of Maryland Center for Environmental Science, P.O. Box 38, Solomons, MD 20688, USA

ARTICLE INFO

Article history:
Received 8 March 2013
Accepted 18 June 2013
Available online 2 July 2013

Keywords:
sediment modeling
Chesapeake Bay
nitrogen
phosphorus
denitrification
silica

ABSTRACT

Sediment-water exchanges of nutrients and oxygen play an important role in the biogeochemistry of shallow coastal environments. Sediments process, store, and release particulate and dissolved forms of carbon and nutrients and sediment-water solute fluxes are significant components of nutrient, carbon, and oxygen cycles. Consequently, sediment biogeochemical models of varying complexity have been developed to understand the processes regulating porewater profiles and sediment-water exchanges. We have calibrated and validated a two-layer sediment biogeochemical model (aerobic and anaerobic) that is suitable for application as a stand-alone tool or coupled to water-column biogeochemical models. We calibrated and tested a stand-alone version of the model against observations of sediment-water flux, porewater concentrations, and process rates at 12 stations in Chesapeake Bay during a 4–17 year period. The model successfully reproduced sediment-water fluxes of ammonium (NH_4^+), nitrate (NO_3^-), phosphate (PO_4^{3-}), and dissolved silica ($Si(OH)_4$ or DSi) for diverse chemical and physical environments. A root mean square error (RMSE)-minimizing optimization routine was used to identify best-fit values for many kinetic parameters. The resulting simulations improved the performance of the model in Chesapeake Bay and revealed (1) the need for an aerobic-layer denitrification formulation to account for NO_3^- reduction in this zone, (2) regional variability in denitrification that depends on oxygen levels in the overlying water, (3) a regionally-dependent solid-solute PO_4^{3-} partitioning that accounts for patterns in Fe availability, and (4) a simplified model formulation for DSi, including limited sorption of DSi onto iron oxyhydroxides. This new calibration balances the need for a universal set of parameters that remain true to biogeochemical processes with site-specificity that represents differences in physical conditions. This stand-alone model can be rapidly executed on a personal computer and is well-suited to complement observational studies in a wide range of environments.

1. Introduction

Sediments are important contributors to the nutrient, oxygen, and carbon cycles of shallow coastal ecosystems. Both autochthonous and allocthonous organic matter deposited to sediments drive sediment biogeochemical processes and resultant nutrient fluxes (Jensen et al., 1990), feed benthic organisms (Heip et al., 1995), and can control sediment oxygen demand (Kemp and Boynton, 1992). In very shallow ecosystems (<5 m), sediments may be populated by submerged vascular plants and/or benthic algal communities, both of which modify sediment biogeochemical reactions via nutrient uptake and sediment oxygenation (Miller et al., 1996; McGlathery et al., 2007). In moderately shallow systems (5–50 m), sediments are sites of organic matter processing, leading to nutrient recycling (Cowan et al., 1996), oxygen consumption (Kemp et al., 1992; Provoost et al., 2013), and associated sediment-water exchange. Therefore, models of sediment diagenetic processes that simulate porewater nutrient concentrations and exchanges of particulate and dissolved substances between the water column and sediments have been

* Corresponding author.
E-mail address: jtesta@umces.edu (J.M. Testa).

0272-7714/$ – see front matter © 2013 Elsevier Ltd. All rights reserved.
http://dx.doi.org/10.1016/j.ecss.2013.06.014

developed (Vanderborght et al., 1977a; Boudreau, 1991; Soetaert and Middelburg, 2009). Such models are valuable tools for understanding and managing nutrients and aquatic resources (Cerco and Cole, 1993).

Sediment process model structures range from relatively simple empirical relationships (Fennel et al., 2006) to more complex process simulations that include time-varying state variables (Boudreau, 1991). Simple model representations include assigning a constant sediment-water flux of O_2 or nutrients (Scully, 2010) or using basic parameterizations of sediment-water flux as a function of overlying water conditions (Imteaz and Asaeda, 2000; Fennel et al., 2006; Hetland and DiMarco, 2008). More complex process models may simulate one or two layers, each of which represent a particular chemical environment (Di Toro, 2001; Emerson et al., 1984; Gypens et al., 2008; Slomp et al., 1998; Vanderborght et al., 1977b). Process models may also resolve depth into numerous layers, allowing for simulations of pore-water constituent vertical profiles (Boudreau, 1991; Dhakar and Burdige, 1996; Cai et al., 2010). Depth resolution in such complex models is usually associated with a higher computational demand (Gypens et al., 2008), thus intermediate complexity formulations (in terms of depth resolution) or simple parameterizations are commonly used when sediment biogeochemical models are coupled to water-column models to simulate integrated biogeochemical processes (Imteaz and Asaeda, 2000; Cerco and Noel, 2005; Sohma et al., 2008; Imteaz et al., 2009), although depth-resolved models have been used for various applications (Luff and Moll, 2004; Reed et al., 2011).

A sediment biogeochemical model was previously developed to link with spatially articulated water-column models describing biogeochemical processes at a limited computational cost (Brady et al., 2013; Di Toro, 2001). This sediment flux model (SFM) separates sediment reactions into two layers to generate fluxes of nitrogen, phosphorus, silica, dissolved oxygen (O_2), sulfide, and methane. SFM has been successfully integrated into water quality models in many coastal systems, including Massachusetts Bay (Jiang and Zhou, 2008), Chesapeake Bay (Cerco and Cole, 1993; Cerco and Noel, 2005), Delaware's Inland Bays (Cerco and Setzinger, 1997), Long Island Sound (Di Toro, 2001), and the WASP model widely used by the United States Environmental Protection agency (Isleib and Thuman, 2011). SFM can also be used as a stand-alone diagnostic tool in sediment process studies, especially over seasonal to decadal time scales (Brady et al., 2013). For example, it has been used to simulate sediment dynamics in the Rhode Island Marine Ecosystem Research Laboratory (MERL) mesocosms (Di Toro, 2001; Di Toro and Fitzpatrick, 1993). Such a stand-alone sediment modeling tool, when combined with high-quality time series observations, can be used for parameter optimization, scenario analysis, and process investigations.

The purpose of this study is: (1) to calibrate and validate a stand-alone version of SFM predictions with a multi-decadal time-series of water-column concentrations and sediment-water exchanges of dissolved inorganic nitrogen, silica, and phosphorus, (2) to utilize SFM to analyze sediment process observations at a range of Chesapeake Bay stations exhibiting differing overlying-water column characteristics (e.g., organic matter deposition rates and oxygen, temperature, and salt concentrations), and (3) to illustrate how SFM can be used to understand processes inferred from field rate measurements. A previous companion paper focused on the ammonium (NH_4^+), O_2, sulfide, and methane modules in SFM (Brady et al., 2013). Here, we focus our process studies on nitrate (NO_3^-), phosphate (PO_4^{3-}), and dissolved silica ($Si(OH)_4$; hereafter DSi) fluxes, as well as denitrification.

2. Methods

SFM was previously calibrated and validated for Chesapeake Bay using sediment-water flux measurements, overlying-water nutrient and O_2 concentrations, and process rates (e.g., denitrification) that were available at that time (1985–1988) for 8 sites (Chapter 14 in Di Toro, 2001). More than two decades later, this study used expanded data availability to re-calibrate and validate SFM, improve its simulation skill for Chesapeake Bay, and demonstrate its utility as a stand-alone tool available for use in other aquatic systems. In this paper we describe and analyze SFM performance in the northern half of Chesapeake Bay using data collected during 4–17 years at 12 stations (Fig. 1). SFM can be run on a personal computer, executing a 25-year run on the time-scale of seconds, and a MATLAB interface is available for input generation, model execution, post-processing, and plotting.

2.1. General model description

The model structure for SFM involves three processes: (1) the sediment receives depositional fluxes of particulate organic carbon and nitrogen, as well as biogenic and inorganic phosphorus and silica, from the overlying water, (2) the decomposition of particulate matter produces soluble intermediates that are quantified as diagenesis fluxes, (3) solutes react, transfer between solid and dissolved phases, are transported between the aerobic and anaerobic layers of the sediment, or are released as gases (CH_4, N_2), and (4) solutes are returned to the overlying water (Fig. 2). The model assumes that organic matter mineralization is achieved by denitrification, sulfate reduction, and methanogenesis, thus aerobic respiration is not explicitly modeled. To model these processes, SFM numerically integrates mass-balance equations for chemical constituents in two functional layers: an aerobic layer near the sediment-water interface of variable depth (H_1) and an anaerobic layer below that is equal to the total sediment depth (10 cm) minus the depth of H_1 (Figs. 2–4). The SFM convention is to use subscripts with "0" when referring to the overlying water, with "1" when referring to the aerobic layer, and with "2" when referring to the anaerobic layer. The simulation time-step is 1 h and output is aggregated at 1-day intervals.

The general forms of the equations are presented in Table 1 (Eqs. (1) and (2)). For example, one can replace C_{T1} with NO_3^- (1) to compute the change in NO_3^- concentration in the aerobic layer (Eq. (1) in Table 1). The governing expressions are mass balance equations that include biogeochemical reactions $\left(\frac{\kappa_1^2}{K_{L01}}C_{T1}\right)$, burial ($\omega_2 C_{T1}$), diffusion of dissolved material between the aerobic sediments and overlying water column ($K_{L01}(f_{d0}C_{T0} - f_{d1}C_{T1})$) and between sediment layers ($K_{L12}(f_{d2}C_{T2} - f_{d1}C_{T1})$), and the mixing of particulate material between layers; ($\omega_{12}(f_{p2}C_{T2} - f_{p1}C_{T1})$). Please refer to Eqs. (1) and (2) in Table 1.

2.2. Aerobic layer depth and surface mass-transfer

The thickness of the aerobic layer, H_1, is solved numerically at each time step of the simulation by computing the product of the diffusion coefficient (D_{O_2}) and the ratio of overlying-water O_2 concentration ($[O_2(0)]$) to sediment oxygen demand (SOD): $H_1 = D_{O_2}\frac{[O_2(0)]}{SOD}$. This relationship has been verified by measurements (Jørgensen and Revsbech, 1985; Cai and Sayles, 1996). The inverse of the second term on the right hand side of Equation (1) is the surface mass transfer coefficient (Eq. (5) in Table 1), which is used as the same mass transfer coefficient for all solutes since differences in the diffusion coefficients between solutes are subsumed in the kinetic parameters that are fit to data (Brady et al., 2013; Di Toro, 2001). It should be noted that in the time varying

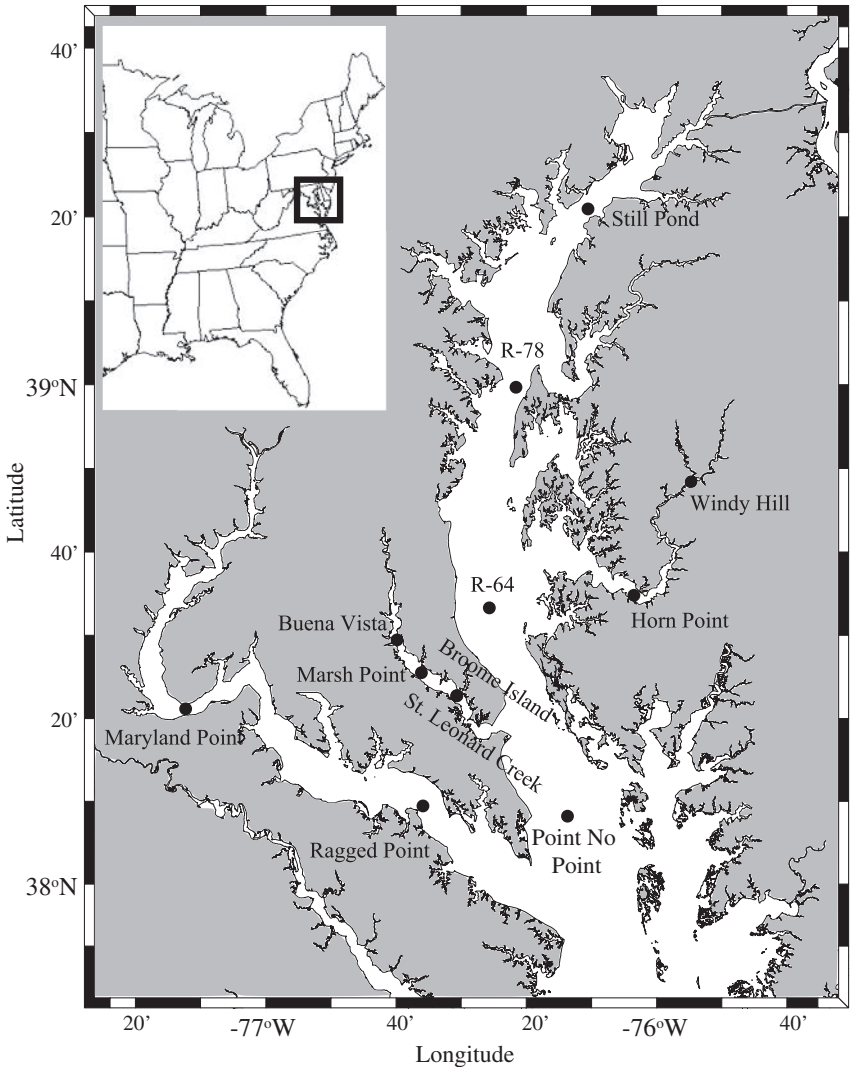

Fig. 1. Map of northern Chesapeake Bay, on the east coast of the United States (inset), showing the locations where Sediment Flux Model (SFM) simulations were compared to Sediment Oxygen and Nutrient Exchange (SONE) observations.

solution, H_1 and H_2 are within the derivative since the depths of the layers are variable, where dynamic entrainment and loss of mass can be quantified (see Chapter 13 in Di Toro, 2001). The depth of the anaerobic layer (H_2) is simply calculated as the difference between total sediment depth (10 cm) and H_1.

2.3. Dissolved and particulate mixing

Dissolved and particle mixing between layers 1 and 2 (K_{L12} and ω_{12}, Eqs. (6) and (7) in Table 1) are modeled as a function of passive transport and proxies that reflect the activities of benthic organisms. K_{L12} enhancement due to benthic faunal activity is parameterized directly, that is, the dissolved mixing coefficient (D_d) is fit to values that typically increase K_{L12} to 2–3 times molecular diffusion (Tables 2 and 3; Gypens et al., 2008; Matisoff and Wang, 1998). The rate of mixing of sediment particles (ω_{12}; Eq. (7) in Table 1) by benthic animals is quantified by estimating the apparent particle diffusion coefficient (D_p; Chapter 13 in Di Toro, 2001). In the model, particle mixing is controlled by temperature (first term in Eq. (7) in Table 1; Balzer, 1996), carbon input (second term in Eq. (7) in Table 1; Robbins et al., 1989), and oxygen (third term in Eq. (7) in Table 1; Díaz and Rosenberg, 1995). To make the model self-consistent, that is to use only internally-computed variables in the parameterizations, the model assumes that benthic biomass and therefore, particle mixing is correlated with the amount of labile carbon (i.e., POC_1) present in the sediment, an assumption that is supported by the literature (Tromp et al., 1995). However, if excess carbon loading creates unfavorable oxygen conditions that reduce macrofaunal density and therefore, bioturbation (Baden et al., 1990), particle mixing is reduced by a term called "benthic stress" (S in Eq. (7) in Table 1). As O_2 decreases, $(1 - k_S S)$ approaches zero. After the stress has passed, the minimum is carried forward for the rest of the year to simulate the observation that benthic communities do not recover until recruitment occurs in the following year (Díaz and Rosenberg, 1995). The mixing parameters used in this model are compared to literature values in Table 3.

2.4. Diagenesis

Diagenesis of particulate organic matter (POM) is modeled by partitioning the settling POM into three reactivity classes, termed the "G model" (Westrich and Berner, 1984). Each class represents a fixed portion of the organic material that reacts at a specific rate (Burdige, 1991). For SFM, three G classes represent three levels of reactivity: G_1 is rapidly reactive (20 day half-life & 65% of settling POM), G_2 is more slowly reactive (1 year half-life & 20% of settling

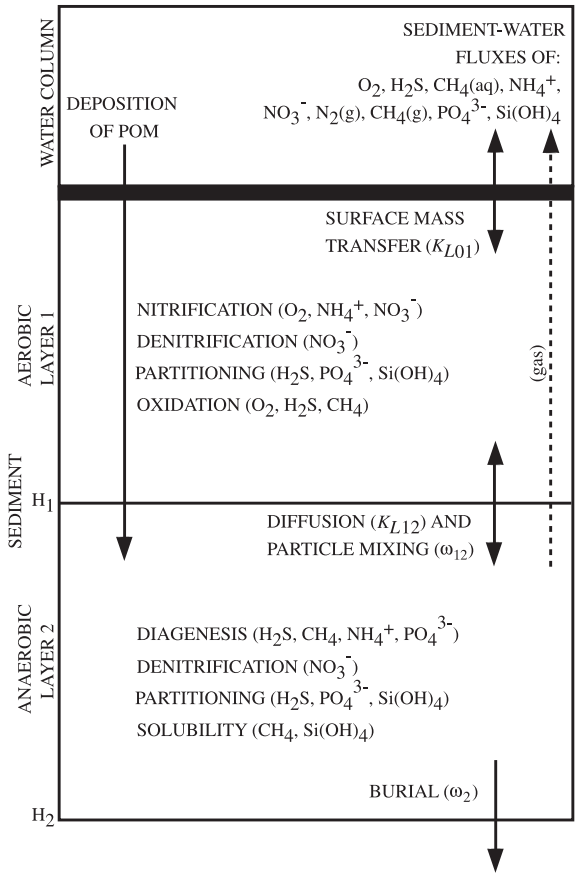

Fig. 2. Generic schematic diagram of the Sediment Flux Model (SFM), including state variables, transport and biogeochemical processes, and boundary conditions. Note that the depths of the aerobic (H_1) and anaerobic (H_2) layers vary over time.

POM), and G_3 (15% of settling POM) is, for this model, non-reactive (see Table 2 for parameters associated with diagenesis and Table 3 for literature ranges). The diagenesis expression is as follows (similar equations govern diagenesis of particulate organic nitrogen and phosphorus):

$$H_2\frac{\mathrm{dPOC}_i}{\mathrm{d}t} = -k_{\mathrm{POC},i}\theta_{\mathrm{POC},i}^{(T-20)}\mathrm{POC}_i H_2 - \omega_2\mathrm{POC}_i + f_{\mathrm{POC},i}J_{\mathrm{POC}} \quad (1)$$

where POC_i is the POC concentration in reactivity class i in the anaerobic layer, $k_{\mathrm{POC},i}$ is the first order reaction rate coefficient, $\theta_{\mathrm{POC},i}$ is the temperature coefficient, ω_2 is the sedimentation velocity, J_{POC} is the depositional POC flux from the overlying water to the sediment, and $f_{\mathrm{POC},i}$ is the fraction of J_{POC} that is in the ith G class. The aerobic layer is not included, due to its small depth relative to the anaerobic layer: $H_1 \approx 0.1$ cm, while $H_2 \approx 10$ cm. Deposition rates for particulate nitrogen (J_{PON}), phosphorus (J_{POP}), and silica (J_{PSi}) are proportional to J_{POC} based on Redfield stoichiometry (Table 2).

Organic matter deposition rates (including particulate biogenic C, N, P, and Si) for each year and station were estimated using a Hooke-Jeeves pattern search algorithm (Hooke and Jeeves, 1961) to minimize the root mean square error (RMSE) between modeled and observed NH_4^+ flux. These estimates of deposition matched well with observations made using several methods and a detailed discussion of this approach is included in a companion paper (Brady et al., 2013).

2.5. Reaction rate formulation

Rate coefficients for aerobic-layer reactions (e.g., nitrification, denitrification, sulfide oxidation, etc.) are relatively similar (Eq. (1) in Table 1). These reactions are modeled to be dependent on the depth of H_1. For example, the nitrification rate expression in the mass balance equations for NH_4^+ is a product of the aerobic layer nitrification rate ($k_{NH_4^+,1}$) and the depth of the aerobic layer (Fig. 3a):

$$k_{NH_4^+,1}H_1 = \frac{D_{NH_4^+}k_{NH_4^+,1}}{K_{L01}} \quad (2)$$

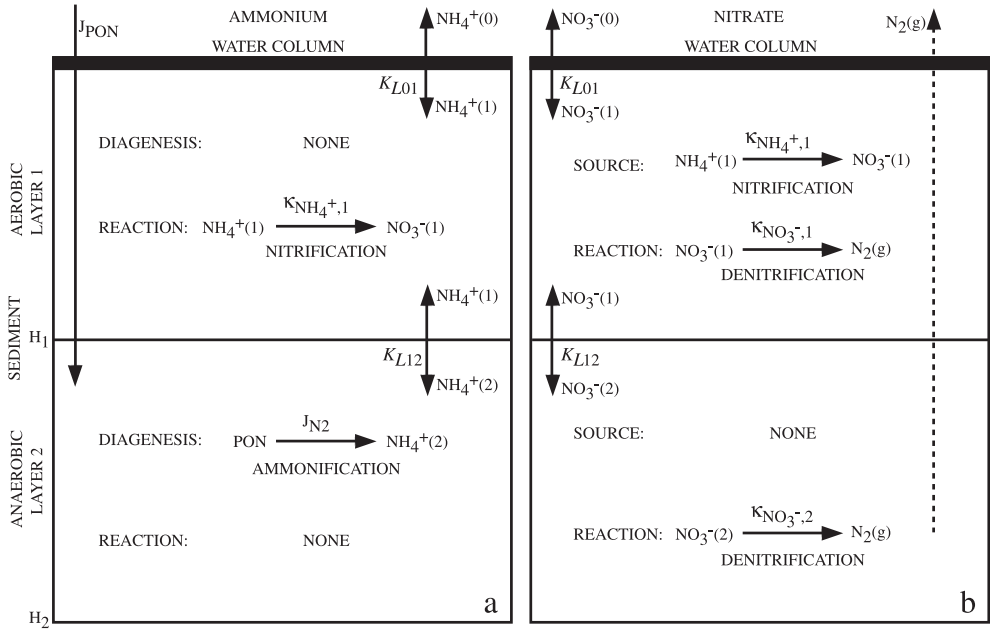

Fig. 3. Schematic representation of nitrogen transport and kinetics in the Sediment Flux Model (SFM). Panels a & b represent the dynamics of the NH_4^+ and NO_3^- models, respectively. Note: (1) there is no diagenesis (ammonification) in layer 1 (panel a). (2) there is no source of NO_3^- in the anaerobic layer, as no O_2 is present (Panel b).

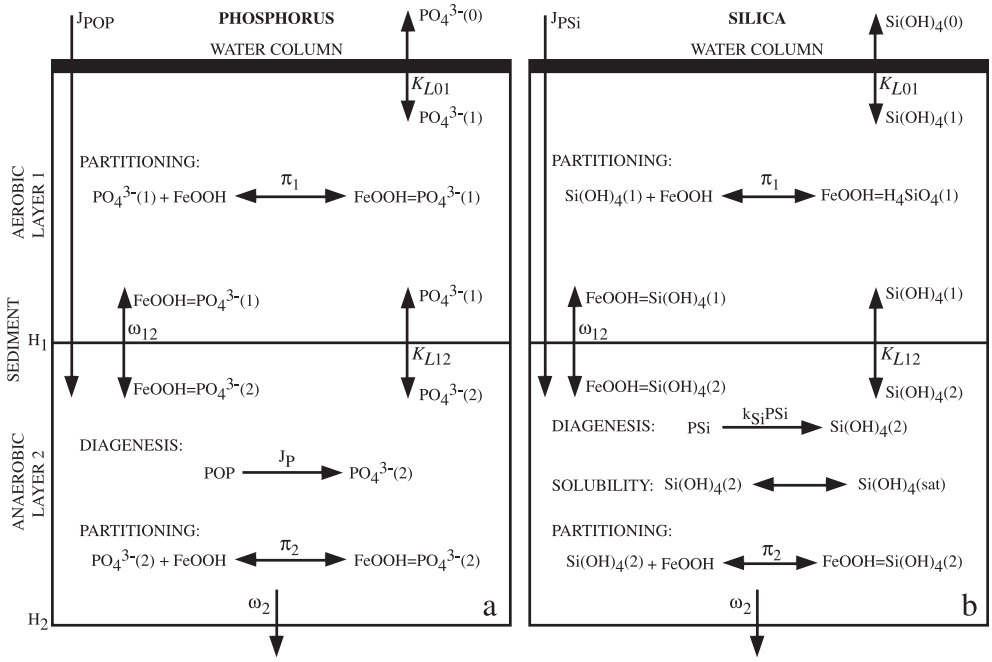

Fig. 4. Schematic representation of the phosphorus and silica transport and kinetics in the Sediment Flux Model (SFM). Panels a and b represent the processes within the phosphorus and silica models, respectively. Note: (1) there is no source of PO_4^{3-} or DSi in the aerobic layer and (2) both PO_4^{3-} and DSi are partitioned between particulate and dissolved phases in both layers, and (3) solubility control for silica dissolution (Panel b).

The product $D_{NH_4^+}k_{NH_4^+,1}$ is made up of two coefficients, neither of which is readily measured. The diffusion coefficient in a millimeter thick layer of sediment at the sediment water interface may be larger than the diffusion coefficient in the bulk of the sediment due to the effects of overlying water shear. It is therefore convenient to subsume two relatively unknown parameters into one parameter that is calibrated to data, called $\kappa_{NH_4^+,1}$ (Fig. 3a):

$$\kappa_{NH_4^+,1} = \sqrt{D_{NH_4^+}k_{NH_4^+,1}} \quad (3)$$

$\kappa_{NH_4^+,1}$ is termed the reaction velocity, since its dimensions are length per time. Squared reaction velocities are then incorporated in the reaction term of the mass balance equations (Table 1).

2.6. Ammonium flux

NH_4^+ concentrations are computed for both aerobic and anaerobic layers via mass balances of biogeochemical and physical processes. Fig. 3a shows the sources and sinks of NH_4^+ in the model. NH_4^+ is produced by organic matter diagenesis (J_{N_2} in Fig. 3a, Eq. (10) in Table 1) in the anaerobic layer, while in the aerobic layer, NH_4^+ is converted to NO_3^- via nitrification using a reaction velocity, $\kappa_{NH_4^+,1}$, (Fig. 3a) with Michaelis–Menten kinetics (Eq. (8) in Table 1). Mass-transfer coefficients are employed to model diffusion of NH_4^+ between the anaerobic and aerobic layers (K_{L12}) and between the aerobic layer and the overlying water (K_{L01}). A more extensive treatment of the NH_4^+ model is given in a companion publication (Brady et al., 2013).

2.7. Nitrate flux

There are two sources of NO_3^- in SFM: (1) NO_3^- enters from the overlying water column as controlled by surface mass transfer (K_{L01}) and the concentration gradient, and (2) NH_4^+ is oxidized in the aerobic layer (i.e., nitrification; Eq. (13) in Table 1, Fig. 3b; see Chapter 4 of Di Toro, 2001). In turn, NO_3^- can be returned to the overlying water column as NO_3^- flux ($J[NO_3^-]$) or converted to nitrogen gas (i.e., denitrification, Eqs. (11) and (12) in Table 1). There is no biogeochemical NO_3^- source in the anaerobic layer (Fig. 3). Although it is conventional to confine denitrification to the anaerobic layer (Gypens et al., 2008), denitrification is modeled in both the aerobic and anaerobic layers in SFM (Fig. 3b). The close coupling between nitrification and denitrification has been suggested by some authors (Blackburn et al., 1994) and there is evidence for denitrification in the oxic layer within anoxic microsites (Jenkins and Kemp, 1984).

2.8. Phosphate flux

The PO_4^{3-} model differs from the nitrogen models in two important ways: (1) there are no reactions for PO_4^{3-} once it is released during diagenesis (Eqs. (14) and (15) in Table 1) and (2) the PO_4^{3-} model includes both organic and inorganic phases (Fig. 4a). There are two sources of PO_4^{3-} to SFM: (1) PO_4^{3-} produced by organic matter diagenesis ($a_{P,C}J_C$ in Fig. 4a, Eq. (16) in Table 1) in the anaerobic layer and (2) PO_4^{3-} that is sorbed onto particles and deposited to sediments (J_{PIP}). Observations of the latter source are scarce, so we initially assumed that sorbed PO_4^{3-} deposition is equivalent to (J_{POP}), which is supported by the observation that POP is roughly 50% of the particulate phosphorus pool in Chesapeake Bay (Keefe, 1994). Because J_{PIP} is likely to be spatially-variable (Keefe, 1994), we optimized J_{PIP} to the sediment-water PO_4^{3-} flux (see below).

Models of phosphorus in marine sediments have traditionally focused on predicting the interstitial concentration of PO_4^{3-} (Van Cappellen and Berner, 1988; Rabouille and Gaillard, 1991), as well as the PO_4^{3-} flux (Slomp et al., 1998; Wang et al., 2003). Because SFM is used to predict sediment-water PO_4^{3-} fluxes, it accounts for the fact that a fraction of the PO_4^{3-} released during diagenesis is trapped in sediments in particulate form via precipitation or sorption to amorphous iron oxyhydroxides (Sundby et al., 1992; Wang et al., 2003). The model also accounts for the dissolution of

iron oxyhydroxides under low oxygen conditions and subsequent release of PO_4^{3-} into porewater (Conley et al., 2002). Thus, the model can account for the temporary storage of PO_4^{3-} near the sediment water interface until oxygen is seasonally-depleted, resulting in iron oxyhydroxides dissolution and subsequently large sediment-water PO_4^{3-} fluxes (Lehtoranta et al., 2009; Testa and Kemp, 2012). SFM distinguishes between solid and dissolved pools of PO_4^{3-} using partition coefficients specific to both layer 1

Table 1
The model equations are listed below. The solutions are found by numerically integrating the equations (Di Toro, 2001). [a]Parameter definitions are located at the bottom of this table.

	Mass balance equations (these are the general equations for C_{T1} and C_{T2}):
1	$\frac{d\{H_1 C_{T1}\}}{dt} = -\frac{\kappa_1^2}{K_{L01}} C_{T1} + K_{L01}(f_{d0} C_{T0} - f_{d1} C_{T1}) + \omega_{12}(f_{p2} C_{T2} - f_{p1} C_{T1}) + K_{L12}(f_{d2} C_{T2} - f_{d1} C_{T1}) - \omega_2 C_{T1} + J_{T1}$
2	$\frac{d\{H_2 C_{T2}\}}{dt} = -\kappa_2 C_{T2} - \omega_{12}(f_{p2} C_{T2} - f_{p1} C_{T1}) - K_{L12}(f_{d2} C_{T2} - f_{d1} C_{T1}) + \omega_2(C_{T1} - C_{T2}) + J_{T2}$
3	where $f_{di} = \frac{1}{1+m_i \pi_i} \quad i = 1, 2$
4	$f_{pi} = 1 - f_{di}$
5	$K_{L01} = \frac{D_{O_2}}{H_1} = \frac{SOD}{[O_2(0)]}$
6	$K_{L12} = \frac{D_d \theta_{D_d}^{(T-20)}}{(H_1+H_2)/2}$
7	$\omega_{12} = \frac{D_p \theta_{D_p}^{(T-20)}}{H_1+H_2} \frac{POC_1}{POC_2} \min_{(\text{each year})}(1 - k_s S)$ where $\frac{dS}{dt} = -k_s S + \frac{K_{M,D_p}}{K_{M,D_p}+[O_2(0)]/2}$
	The kinetic and source terms for the ammonium, nitrate, phosphate, and silica systems are listed next.
	Ammonium (NH_4^+)
8	$\kappa_1^2 = \kappa^2_{NH_4^+,1} \theta^{(T-20)}_{NH_4^+} \left(\frac{K_{M,NH_4^+} \theta^{(T-20)}_{K_{M,NH_4^+}}}{K_{M,NH_4^+} \theta^{(T-20)}_{K_{M,NH_4^+}} + [NH_4^+(1)]} \right) \left(\frac{[O_2(0)]/2}{K_{M,NH_4^+,O_2} + [O_2(0)]/2} \right)$
9	$\kappa_2 = 0$
10	$J_{T1} = 0$ and $J_c = \sum_{i=1}^{2} -k_{POC,i} \theta^{(T-20)}_{POC,i} POC_i H_2$ $J_{T2} = a_{N,C} J_c$
	Nitrate (NO_3^-)
11	$\kappa_1^2 = \kappa^2_{NO_3^-,1} \theta^{(T-20)}_{NO_3^-}$
12	$\kappa_2 = \kappa_{NO_3^-,2} \theta^{(T-20)}_{NO_3^-}$
13	$J_{T1} = \kappa^2_{NH_4^+,1} \theta^{(T-20)}_{NH_4^+} \frac{[NH_4^+(1)]}{K_{L01}} \left(\frac{K_{M,NH_4^+} \theta^{(T-20)}_{K_{M,NH_4^+}}}{K_{M,NH_4^+} \theta^{(T-20)}_{K_{M,NH_4^+}} + [NH_4^+(1)]} \right) \left(\frac{[O_2(0)]/2}{K_{M,NH_4^+,O_2} + [O_2(0)]/2} \right)$ $J_{T2} = 0$
	Phosphate (PO_4^{3-})
14	$\kappa_1^2 = 0$
15	$\kappa_2 = 0$
16	$J_{T1} = 0$ and $J_{T2} = a_{P,C} J_C + J_{PIP}$
	Particulate Silica (P_{Si})
17	$\frac{d\{H_2[P_{Si}]\}}{dt} = -S_{Si} H_2 - \omega_2 [P_{Si}(2)] + J_{PSi} + J_{\text{Detrital}_{Si}}$
18	$S_{Si} = k_{Si} \theta^{(T-20)}_{Si} \frac{[P_{Si}(2)]}{K_{M,P_{Si}} + [P_{Si}(2)]} (Si_{\text{sat},20} \theta^{(T-20)}_{Si} - f_{d2}[Si(OH)_4(2)])$ $J_{PSi} = a_{Si,C} J_C$
	$J_{Detr_{Si}} = \text{Non-algal particulate } J_{PSi} \text{ flux}$
	Silicate ($Si(OH)_4$)
19	$\kappa_1^2 = 0$
20	$\kappa_2 = 0$
21	$J_{T1} = 0$ $J_{T2} = k_{Si} \theta^{(T-20)}_{Si} \frac{[P_{Si}(2)]}{K_{M,PSi} + [P_{Si}(2)]} (Si_{\text{sat},20} \theta^{(T-20)}_{Si_{\text{sat}}} - f_{d2}[Si(OH)_4(2)] H_2)$

Table 1 (*continued*)

	Mass balance equations (these are the general equations for C_{T1} and C_{T2}):
	Partitioning: PO_4^{3-} *nd* $Si(OH)_4$
22	*If* $[O_2(0)] < [O_2]_{critPO_4^{3-},Si}$:
	$\pi_{PO_4^{3-},Si,1} = \pi_{PO_4^{3-},Si,2} \Delta\pi_{PO_4^{3-},Si,1} \frac{[O_2(0)]}{[O_2]_{critPO_4^{3-},Si}}$
	If $[O_2(0)] \geq [O_2]_{critPO_4^{3-},Si}$:
	$\pi_{PO_4^{3-},Si,1} = \pi_{PO_4^{3-},Si,2}\ \Delta\pi_{PO_4^{3-},Si,1}$

[a] H_1, H_2 = depth of layer 1 and 2 (cm); C_{T0}, C_{T1}, C_{T2} = total (dissolved + particulate) concentration in layers (mmol m^{-3}); POC_1 = Layer 1 particulate organic carbon concentration (mmol m^{-3}), POC_R = reference particulate organic carbon concentration (0.1 mg C g solids^{-1}); f_{d1}, f_{d2} = dissolved fraction of total concentration in each layer; f_{p1}, f_{p2} = particulate fraction of total concentration in each layer; K_{L12} = mass transfer coefficient between layers 1 and 2; K_{L01} = ratio of SOD to overlying water dissolved O_2, or mass transfer coefficient between layer 1 and the overlying water-column; K_{L12} = mass transfer coefficient between layer 1 and 2 (m d^{-1}); ω_2 = sedimentation velocity (cm y^{-1}); ω_{12} = particle mixing velocity between layers 1 and 2 (m d^{-1}); k_s = first-order decay coefficient for accumulated benthic stress (d^{-1}); S = benthic stress term (d); J_{T1} = source of solute to layer 1 (mmol m^{-2} d^{-1}); J_{T2} = source of solute to layer 2 (mmol m^{-2} d^{-1}); κ_1, κ_2 = reaction velocity for first-order removal reaction rate constant in layer 1 and 2 (m d^{-1}); m_1, m_2 = solids concentration in layer 1 and 2 (kg L^{-1}); π_1, π_2 = partition coefficient in layer 1 and 2 (L kg^{-1}); D_p = diffusion coefficient of particulate solutes due to particle mixing (cm^2 d^{-1}); D_d = diffusion coefficient of dissolved solutes (cm^2 d^{-1}); $\theta_{D_{p,d}}$ = temperature coefficient for D_p or D_d; $K_{M,i}$ = half saturation coefficient (i = relevant parameter or variable, in concentrations units of relevant variable); $a_{N,C}$ = stoichiometric ratio of NH_4^+ released to POC mineralized (mol N mol C^{-1}); $a_{Si,C}$ = stoichiometric ratio of $Si(OH_4)$ released to POC mineralized (mol O_2 mol C^{-1}). Where specific solutes are shown (e.g. $[NO_3^-(i)]$), i = layer). Parameter values listed in Table 2. C_{T1} and C_{T2} were computed for NH_4^+, NO_3^-, PO_4^{3-} (=dissolved + particulate phosphate), and $Si(OH_4)$ (=dissolved + particulate silica). $[O_2]_{critPO_4^{3-},Si}$ is the O_2 concentration below which the aerobic layer partition coefficient is a function of O_2.

and 2 (Eqs. 3 and 4 in Table 1). The partition coefficient in layer 1 is larger than in layer 2 under oxic conditions, representing the higher concentration of oxidized Fe and allowing for PO_4^{3-} trapping. Once oxygen falls below a critical concentration (Eq. (22) in Table 1, Table 2), a larger fraction of the total PO_4^{3-} is transitioned to the dissolved pool.

Table 2
Sediment flux model parameters.

Variable	Value	Units	Variable	Value	Units
Recycle fractions			Benthic stress		
$f_{POC,N,P,1}$	0.65		k_S	0.03	d^{-1}
$f_{POC,2}$	0.20		$K_{M,Dp}$	62.5	μM O_2*
$f_{PON,2}$	0.25		Ammonium		
$f_{POP,2}$	0.20		$\kappa_{NH_4^+,1}$	0.131	m d^{-1}
$f_{POC,3}$	0.15		$\theta_{NH_4^+}$	1.123	
$f_{PON,3}$	0.10		K_{M,NH_4^+}	52.0	μM N
$f_{POP,3}$	0.15		$\theta_{K_{M,NH_4^+}}$	1.125	
Diagenesis			$K_{M,NH_4^+O_2}$	11.5	μM O_2
$k_{POC,N,P,1}$	0.01†	d^{-1}	a_{O_2,NH_4^+}	2.0	mol O_2 mol^{-1} N
$\theta_{POC,N,P,1}$	1.10		Nitrate		
$k_{POC,N,P,2}$	0.0018	d^{-1}	$\kappa_{NO_3^-,1}$	0.10–0.30‡	m d^{-1}
$\theta_{POC,N,P,2}$	1.15		$\kappa_{NO_3^-,2}$	0.25	m d^{-1}
k_{Si}	0.5	d^{-1}	$\theta_{NO_3^-}$	1.08	
θ_{Si}	1.10		a_{O_2,NO_3^-}	1.25	mol O_2 mol^{-1} N
$a_{O_2,C}$	1.0	mol O_2 mol^{-1} C	Silica		
$a_{N,C}$	0.167	mol N mol^{-1} C	$Si_{sat,20}$	1390	mmol Si m^{-3}
$a_{P,C}$	0.009	mol P mol^{-1} C	$\theta_{Si_{sat}}$	1.023	
$a_{Si,C}$	0.171	mol Si mol^{-1} C	$K_{M,PSi}$	3560	mmol Si m^{-3}
Solids			$\Delta\pi_{Si,1}$	5–15§	L kg^{-1}
ω_2	0.7	cm y^{-1}	$\pi_{Si,2}$	15–50§	L kg^{-1}
m_1	0.50	kg L^{-1}	$J_{Detr_{Si}}$	1.8	mmol Si m^{-2} d^{-1}
m_2	0.50	kg L^{-1}	$[O_2]crit_{Si}$	62.5	μM O_2
Mixing			Phosphate		
D_d	5.0	cm^2 d^{-1}	$\Delta\pi_{PO_4^{3-},1}$	100–300§	L kg^{-1}
θ_{Dd}	1.08		$\pi_{PO_4^{3-},2}$	50–100§	L kg^{-1}
D_p	0.6	cm^2 d^{-1}	$[O_2]crit_{PO_4^{3-}}$	62.5	μM O_2
θ_{Dp}	1.117		Dimensions		
POC_R	0.1	mg C g solids^{-1}	$H_1 + H_2$	10.0	cm

* Indicates that units are in O_2 equivalents.
† Value was 0.035 in the original calibration.
‡ Denitrification reaction velocity range reflects the range of values from the original calibration and optimization routine.
§ Partitioning coefficient range reflects the range of values from the optimization routine.

2.9. Dissolved silica flux

The DSi model includes the same partitioning formulation (including O_2-dependency) as the PO_4^{3-} model (Eq. (22) in Table 1) and also has no reactions in layer 1 and 2 (Eqs. 17 and 18 in Table 1, Fig. 4b). Similar partitioning formulations are absent from previous silica models Vanderborght et al., 1977a, but are present in more recent formulations (Rabouille and Gaillard, 1990), based upon evidence for DSi sorption to Fe oxyhydroxides (Sigg and Stumm, 1981), which hereafter will be referred to as FeOOH.

Unlike phosphorus, nitrogen and carbon, silica diagenesis is a dissolution reaction rather than a microbially-mediated respiratory process. The particulate silica deposited to sediments that may be dissolved originates from two sources: (1) biogenic silica in diatom algal material (J_{PSi}) and (2) detrital silica associated with terrestrially-derived particles ($J_{Detr_{Si}}$, Eqs. (17) and (18) in Table 1, Table 2). Silica dissolution has been found to be a function of the degree of undersaturation, pH, temperature, particulate silica concentration, salinity, and the nature of the surfaces of the solid-phase silica (Conley et al., 1993; Van Cappellen and Linqing, 1997b; Yamada and D'Elia, 1984). In SFM, the diagenesis of particulate silica is a function of a first-order rate constant (k_{Si}) with a temperature dependency (θ_{Si}), a Michaelis–Menten dependency on particulate silica (P_{Si}), and a first-order dependency on the degree of undersaturation (Eq. (18) in Table 1, Table 2). The original calibration of SFM considered silica solubility to be independent of temperature (Di Toro, 2001). In this analysis, a temperature dependency on silica solubility was added (Eq. (18) in Table 1), as has been suggested in the literature (Lawson et al., 1978; Van Cappellen and Linqing, 1997a). Comparisons of the other model silica parameters with associated literature values are provided in Table 3.

2.10. Overlying water concentrations

Data for overlying water-column nutrient and O_2 concentrations nearest the sediment-water interface in Chesapeake Bay, which are required boundary conditions for the stand-alone SFM simulations,

Table 3
Comparison of sediment flux model parameters to literature parameters.

SFM parameter	Units	SFM value	Literature range	Citations
Diagenesis				
$k_{POC,N,P,1}$	d^{-1}	0.01–0.035	0.019–0.066	(a)
$\theta_{POC,N,P,1,2}$		1.10	1.052–1.166	(b)
$k_{POC,N,P,2}$	d^{-1}	0.0018	0.0012–0.0088	(c)
Ammonium				
$\theta_{K_{M,NH_4^+}}$		1.125	1.125	(d)
$\kappa_{NH_4^+,1}$	m d^{-1}	0.131	*n/a*	(e)
$\theta_{NH_4^+}$		1.123	1.076–1.127	(f)
K_{M,NH_4^+}	μM N	52	24–85	(g)
$K_{M,NH_4^+O_2}$	μM O_2	11.5	1.0–62.5	(h)
Silica				
k_{Si}	d^{-1}	0.5	0.02–0.2*	(i)
θ_{Si}		1.10	1.059–1.084	(j)
$Si_{sat,20}$	mmol Si m^{-3}	1390	946–1560	(k)
$K_{M,PSi}$	mmol Si m^{-3}	3560	707–3571	(l)
Nitrate				
$\kappa_{NO_3^-,1,2}$	m d^{-1}	0.1–0.3	*n/a*	(m)
$\kappa_{NO_3^-,1g}$	m d^{-1}	0.2	*n/a*	(n)
$\theta_{NO_3^-}$		1.08	1.056–1.20	(o)
Transport				
ω_2	cm y^{-1}	0.7	0.02–1.0	(p)
D_d	cm^2 d^{-1}	5.0	0.6–8.64†	(q)
θ_{Dd}		1.08	1.08	(r)
D_p	cm^2 d^{-1}	0.6	<0.001–0.5‡	(s)
θ_{Dp}		1.117	1.07–1.117	(t))

(a) Soetaert et al., 1996a, Westrich and Berner, 1984, Roden and Tuttle, 1996, Burdige, 1991; (b) Klump and Martens, 1989, Wheatland, 1954, Kaplan and Rittenberg, 1964, Nedwell and Floodgate, 1972, Vosjan, 1974, Goldhaber et al., 1977, Jørgensen, 1977), Abdollahi and Nedwell, 1979, Westrich and Berner, 1988; (c) Grill and Richards, 1964, Otsuki and Hanya, 1972, Westrich and Berner, 1984, Turekian et al., 1980, Billen, 1982, Roden and Tuttle, 1996; (d) all reported values are the same; Stevens et al., 1989, Young et al., 1979, (e) comparable parameters not reported in literature; (f) Antoniou et al., 1990, Argaman and Miller, 1979, Painter and Loveless, 1983, Stevens et al., 1989, Warwick, 1986, Young et al., 1979, Henriksen and Kemp, 1988; (g) Argaman and Miller, 1979, Cooke and White, 1988, Gee et al., 1990, Shieh and LaMotta, 1979, Stevens et al., 1989, Young et al., 1979, Henriksen and Kemp, 1988; (h) Soetaert et al., 1996a, Stenstrom and Poduska, 1980; (i) Vanderborght et al., 1977a, Di Toro, 2001, Ullman and Aller, 1989, Lawson et al., 1978; (j) Di Toro, 2001, Conley and Schelske, 1989, Lawson et al., 1978; (k) Di Toro, 2001, Ullman and Aller, 1989, Lawson et al., 1978, Rickert et al., 2002; (l) Di Toro, 2001, Conley et al., 1986; (m-n) comparable parameters not reported in literature; (o) Argaman and Miller, 1979, Lewandoswki, 1982, Messer and Brezonik, 1984, Nakajima et al., 1984; (p) Vanderborght et al., 1977a, Jahnke et al., 1982, Wang et al., 2003; (q) Wang et al., 2003, Krom and Berner, 1980, Vanderborght et al., 1977a, Emerson et al., 1984, Billen, 1982, Soetaert et al., 1996b – note that this value may be depth-dependent; (r) Wang et al., 2003, based on Di Toro, 2001; (s) Wang et al., 2003, Beauchard et al., 2012, Balzer, 1996; (t) Gerino et al., 1998, Wang et al., 2003.

* Some reported values are much lower (see discussion).

† Range includes measured and computed rates; molecular diffusion coefficients for SFM variables range from 0.66–1.97.

‡ Range reflects measured values that include the effects of temperature and benthic biomass.

were retrieved for each station and date from the Chesapeake Bay Program (CBP) Water Quality database (http://www.chesapeakebay.net/data_waterquality.aspx). Measurements of bottom water salinity, dissolved O_2, NH_4^+, NO_3^-, and PO_4^{3-} made as part of the Sediment Oxygen and Nutrient Exchange (SONE) experiments (Boynton and Bailey, 2008) were augmented by CBP data by combining the time series and using piecewise cubic hermite interpolation (PCHIP) to derive daily overlying water-column values. DSi data were only available in the CBP dataset. The fine temporal resolution of the combined SONE and CBP monitoring time series insures that the onset of hypoxia and winter temperature regimes (not measured in the SONE dataset) were properly simulated. To calculate initial sediment nutrient conditions, the time series of POM deposition and overlying water concentrations were repeated until there was 15 years of input. The synthetic 15 year time series was used as the model input, followed by the years with observations. This insures that the initial conditions for SFM particulate and dissolved constituents are consistent with the depositional fluxes and parameters.

2.11. Calibration and validation datasets

Observed sediment-water fluxes of NH_4^+, nitrite + nitrate ($NO_2^- + NO_3^-$), PO_4^{3-}, and DSi were estimated from time-course changes in constituents during incubations of intact plexiglass sediment cores (Boynton and Bailey, 2008). Although not presented in this paper, the organic matter deposition rates used in this analysis were validated against available observations, as were rates of sediment oxygen demand, sulfate reduction, and porewater concentrations (Brady et al., 2013). Cores for the measurement of sediment denitrification were collected by box coring in both the upper Chesapeake Bay ("Still Pond") and in the mid-bay ("R-64"); the methods for core incubation are described in detail elsewhere (Kana et al., 2006). Briefly, triplicate cores from each site that had aerobic overlying water conditions were bubbled with air for ~2 h while submersed in a temperature controlled bath. Tops caps with suspended magnetic stirrers were attached and time courses of solute (NH_4^+, $NO_2^- + NO_3^-$) and gas (O_2, N_2, Ar) concentrations were determined. The rate of gas flux was determined from high precision N_2:Ar or O_2:Ar ratios using membrane inlet mass spectrometry. While the fluxes of N_2 are referred to as denitrification, they are actually the summation of all gaseous N transformation processes and may include processes such as anammox (Rich et al., 2008) or N fixation associated with sulfate reduction (Bertics et al., 2013); fluxes of N_2O were not measured.

2.12. Error metrics and parameter optimization

Model-data comparisons were facilitated using multiple skill assessment metrics (Stow et al., 2009). RMSE, mean error (sum of residuals divided by the number of observations), and reliability index (RI) were computed for each flux/station combination. Mean error is a measure of aggregate model bias while RMSE takes into account the magnitude of model-data discrepancies. Finally, the RI quantifies the average factor by which model predictions differ from observations. An RI of 2, for instance, would indicate that SFM predicts the observation within a factor 2, on average (Stow et al., 2009).

We first ran SFM at 12 stations for all years where observations of sediment-water fluxes were available using the parameter set from the original calibration of SFM in Chesapeake Bay (Di Toro, 2001). We then calibrated several components of the model to optimize model-data fits. Specifically, we ran 50 simulations with 50 different values for 10 parameters to find the minimum root mean square error (RMSE) between modeled and observed solute fluxes for the nutrient flux (NO_3^-, PO_4^{3-}, and DSi) associated with each parameter. This optimization routine requires the range of potential parameter values and the number of simulations to be run using parameter values equally spaced between the range. The pattern search range for each parameters was centered around the parameter value from the original model calibration (Di Toro, 2001). This process is repeated for each station and the RMSE for each variable (e.g., $J[NO_3^-]$) and parameter (e.g., $\kappa_{NO_3^-,1}$) is saved after each run. Parameter ranges were constrained in each case based on published values and chosen after careful consideration of model-data residuals. Optimization simulations were performed for 10 parameters, which is a subset of the total parameter set, including: (1) the aerobic and anaerobic layer denitrification reaction velocity ($\kappa_{NO_3^-,1}$, $\kappa_{NO_3^-,2}$), (2) the PO_4^{3-} and DSi partition coefficients in layer 1 and 2 ($\Delta\pi_{PO_4^{3-},1}$, $\pi_{PO_4^{3-},2}$, $\Delta\pi_{Si,1}$, $\pi_{Si,2}$), (3) the

particulate inorganic PO_4^{3-} and DSi depositional fluxes, (4) the half-saturation constant for P_{Si} dependency of silica dissolution ($K_{M,PSi}$), and (5) the first-order silica diagenesis rate constant (k_{Si}).

3. Results

3.1. Sediment-water nitrogen fluxes

Using the original model calibration, which was based on measurements made during 1985–1988, SFM sediment-water NO_3^- fluxes matched observations at three sites with similar characteristics (e.g., Still Pond in Fig. 5a), but under-estimated net influxes to sediments at other sites (e.g., R-64 in Fig. 5b, Table 4). Specifically, SFM simulated NO_3^- fluxes well at sites with low salinity, in close proximity to freshwater discharges from major river, and relatively high (normoxic) O_2 levels throughout the year (Windy Hill, Still Pond, and Maryland Point; Table 4). However, at the other nine sites, which are generally deeper and experience seasonal hypoxia and anoxia, the original SFM calibration was unable to capture the large spring NO_3^- fluxes into the sediment that occurred in years after 1988 (e.g., Fig. 5b, Table 4).

The parameter optimization routine to minimize the RMSE between observed and modeled NO_3^- fluxes yielded different results for the aerobic and anaerobic denitrification velocity ($\kappa_{NO_3^-,1}$ and $\kappa_{NO_3^-,2}$). Although model results were relatively insensitive to changes in the anaerobic-layer denitrification velocity (data not shown), alterations of the aerobic-layer denitrification velocity resulted in substantial improvements in the NO_3^- flux predictions across the nine relatively hypoxic sites (Fig. 5c, Table 4). The value of $\kappa_{NO_3^-,1}$ from the original calibration (0.1 m d^{-1}) resulted in the lowest RMSE at Windy Hill, Still Pond, and Maryland Point (low salinity, normoxic), while higher values of $\kappa_{NO_3^-,1}$ reduced RMSE at the other sites (higher salinity, seasonally-hypoxic; Fig. 5c, Table 4). Increasing the denitrification velocity 2–4 times more than the original calibration resulted in a 38% reduction in RMSE across hypoxic sites (Table 4). Importantly, the optimized value of $\kappa_{NO_3^-,1}$ correlated significantly ($r = -0.81$, $p = 0.002$) with the model-computed depth of the aerobic layer (Fig. 5c inset).

We restructured the formulation for denitrification to make it uniform across varying environmental conditions. The strong correlation between H_1 and optimized $\kappa_{NO_3^-,1}$ (Fig. 5c inset) indicates that the depth-dependence of aerobic layer NO_3^- removal (via denitrification) is responsible for the station specific optimization of $\kappa_{NO_3^-,1}$. In the NO_3^- mass balance, the squared aerobic layer denitrification velocity ($\kappa_{NO_3^-,1}$) is divided by the surface mass-transfer coefficient (K_{L01}; Eq. (1) in Table 1). Because $\kappa_{NO_3^-,1} = \sqrt{D_{NO_3^-}\, k_{NO_3^-,1}}$ and $K_{L01} = \frac{D_{NO_3^-}}{H_1}$, the NO_3^- removal term is $(D_{NO_3^-}\, k_{NO_3^-,1}) \cdot \left(\frac{D_{NO_3^-}}{H_1}\right)^{-1} [NO_3^-(1)]$, or in a more simplified form, $k_{NO_3^-,1} \cdot H_1 \cdot [NO_3^-(1)]$. This formulation implies that denitrification is occurring uniformly over the depth of the aerobic layer, yet if anaerobic microsites are unequally distributed, or denitrification occurs only at the interface of the aerobic and anaerobic layers, this implication would not be valid. Thus, we executed a second optimization without the depth dependence, where aerobic-layer denitrification is simply $k_{NO_3^-,1} \cdot [NO_3^-(1)]$. The results of this second optimization indicated that a spatially invariant denitrification velocity of 0.2 m d^{-1}, which we call $k_{NO_3^-,1g}$, resulted in an overall 33% decrease in RMSE across all observations at all sites (Fig. 6, Table 4).

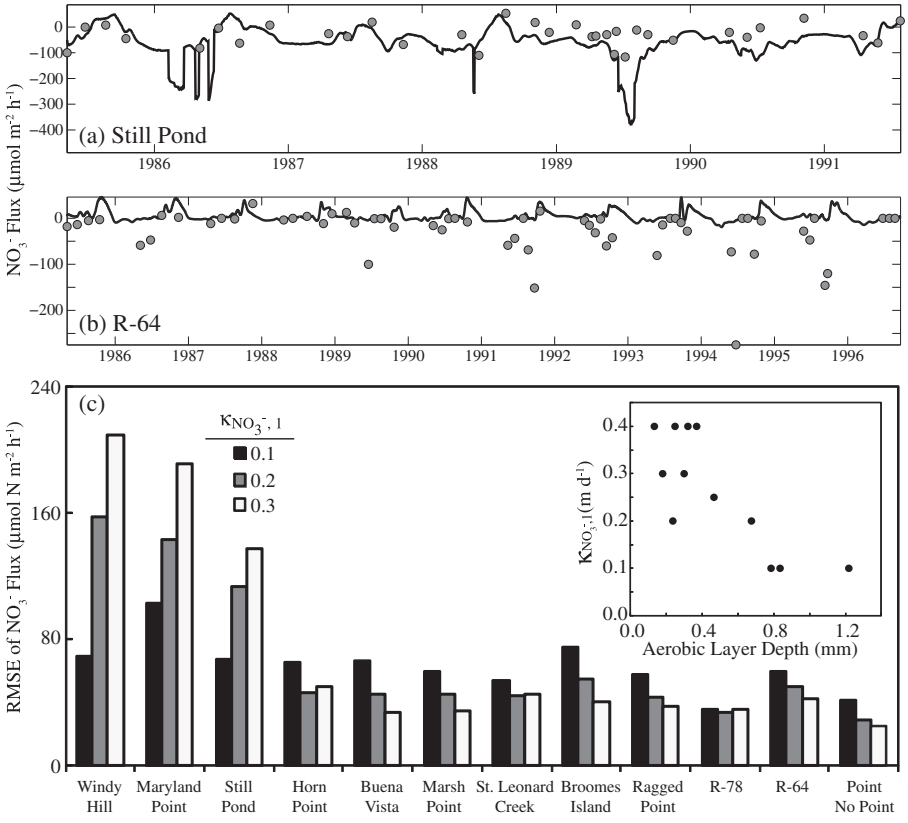

Fig. 5. Modeled (lines) versus observed (circles) sediment-water NO_3^- flux at Still Pond (a) and R-64 (b), where aerobic-layer denitrification was modeled using a layer 1 denitrification velocity ($kNO_3^-,1$) of 0.1 m day^{-1} from the original calibration. (c) Comparison of RMSE values for modeled NO_3^- flux across all stations at varying values of the aerobic-layer denitrification velocity, where the optimized value for $kNO_3^-,1$ is highly correlated to model-computed aerobic-layer depth across stations (inset).

Table 4
Root mean square error (RMSE), reliability index (RI), and mean error (ME) for model-data comparison of sediment-water nitrate, phosphate and silicate fluxes. Station depth (m), mean annual salinity, and summer (June–August) O_2 (μM) in bottom-water included for each station. Refer to text for model and parameterization schemes and to Brady et al. (2013) for station location details.

Sites	$J[NO_3^-]$ (μmol N m^{-2} h^{-1})				$J[PO_4^{3-}]$ (μmol P m^{-2} h^{-1})			J[Si] (μmol Si m^{-2} h^{-1})		
	Metric	Original calibration	$\kappa_{NO_3^-,1}$ optimized by station	$k_{NO_3^-,1g}$ optimized for all stations	Original calibration	$\Delta\pi PO_4^{3-}$ optimized by salinity	Optimized model	Original calibration	Temperature dependent solubility	Partitioning reduced
Windy Hill	RMSE	23.44	19.34	38.88	18.11	14.18	13.27	276.55	275.48	166.52
Salinity = 1.0	RI	1.29	1.27	1.33	1.88	1.78	1.82	1.66	1.69	1.29
O_2 = 183.1	ME	5.62	−7.67	27.59	9.01	1.42	−2.65	159.23	161.34	50.35
Maryland Point	RMSE	32.32	32.21	43.91	10.24	10.24	10.24	206.66	207.73	183.59
Salinity = 1.9	RI	1.22	1.22	1.33	1.38	1.38	1.38	1.43	1.43	1.39
O_2 = 196.8	ME	1.98	5.62	28.02	−1.11	−1.11	−1.11	45.46	43.26	35.46
Still Pond	RMSE	23.32	21.89	33.53	3.20	3.20	3.20	144.12	144.99	148.29
Salinity = 4.8	RI	1.18	1.18	1.30	1.21	1.21	1.21	1.78	1.78	1.76
O_2 = 167.4	ME	10.75	3.71	23.85	−0.62	−0.62	−0.62	84.51	83.81	11.59
Horn Point	RMSE	21.06	15.01	13.04	42.44	32.71	27.08	394.40	391.92	216.21
Salinity = 11.1	RI	1.21	1.15	1.15	1.62	1.76	1.83	1.62	1.65	1.27
O_2 = 150.4	ME	−11.83	2.71	1.08	−7.31	−11.04	−12.86	282.60	279.96	118.01
Buena Vista	RMSE	20.67	10.11	9.38	34.28	28.52	26.05	419.70	411.15	225.46
Salinity = 11.5	RI	1.21	1.12	1.13	1.33	1.30	1.32	1.49	1.48	1.25
O_2 = 107.6	ME	−14.16	2.59	−2.73	19.22	9.24	3.86	345.67	341.94	124.18
Marsh Point	RMSE	20.61	10.54	11.06	48.73	39.41	34.00	306.66	306.01	179.15
Salinity = 13.2	RI	1.17	1.11	1.13	1.47	1.56	1.84	1.86	1.85	1.23
O_2 = 54.8	ME	−14.43	0.29	−2.89	1.55	1.84	1.42	153.42	151.64	14.51
St. Leonard Creek	RMSE	18.13	14.76	12.42	11.89	12.22	12.98	346.03	345.33	211.19
Salinity = 13.6	RI	1.17	1.15	1.12	1.29	1.44	1.47	1.85	1.87	1.29
O_2 = 94.2	ME	−10.09	0.88	0.71	2.27	−2.85	−5.96	268.37	267.81	108.48
Broome Island	RMSE	24.79	11.32	13.34	52.58	35.13	26.17	309.26	307.91	188.14
Salinity = 13.8	RI	1.25	1.15	1.18	1.70	1.62	1.58	1.67	1.68	1.34
O_2 = 75.7	ME	−19.00	1.12	−6.21	−5.06	−6.82	−8.02	204.26	202.50	58.75
Ragged Point	RMSE	19.67	12.73	11.59	23.91	18.92	14.86	204.50	198.99	124.76
Salinity = 15.6	RI	1.23	1.19	1.16	1.38	1.48	1.68	1.78	1.77	1.22
O_2 = 27.5	ME	−11.07	−0.36	−1.52	−6.08	−5.07	−4.64	80.12	79.41	−14.65
R-78	RMSE	11.76	11.26	9.02	11.70	11.33	11.05	158.14	158.14	107.86
Salinity = 17.0	RI	1.46	1.37	1.20	1.48	1.76	1.75	1.77	1.77	1.28
O_2 = 17.5	ME	−3.26	2.32	2.08	2.24	1.68	1.41	107.14	107.14	41.42
R-64	RMSE	20.10	12.48	10.84	20.27	16.64	12.84	267.94	267.98	183.32
Salinity = 19.3	RI	1.17	1.13	1.13	1.32	1.42	1.42	1.73	1.72	1.24
O_2 = 14.9	ME	−12.17	0.74	−4.22	−6.35	−4.48	−3.81	188.37	187.82	109.21
Point No Point	RMSE	14.04	8.38	7.08	13.38	10.56	9.42	260.48	260.48	173.13
Salinity = 20.6	RI	1.25	1.14	1.15	1.27	1.29	1.29	1.96	1.96	1.36
O_2 = 36.9	ME	−10.10	−0.70	−3.36	−5.18	−5.24	−5.54	224.56	224.56	114.17

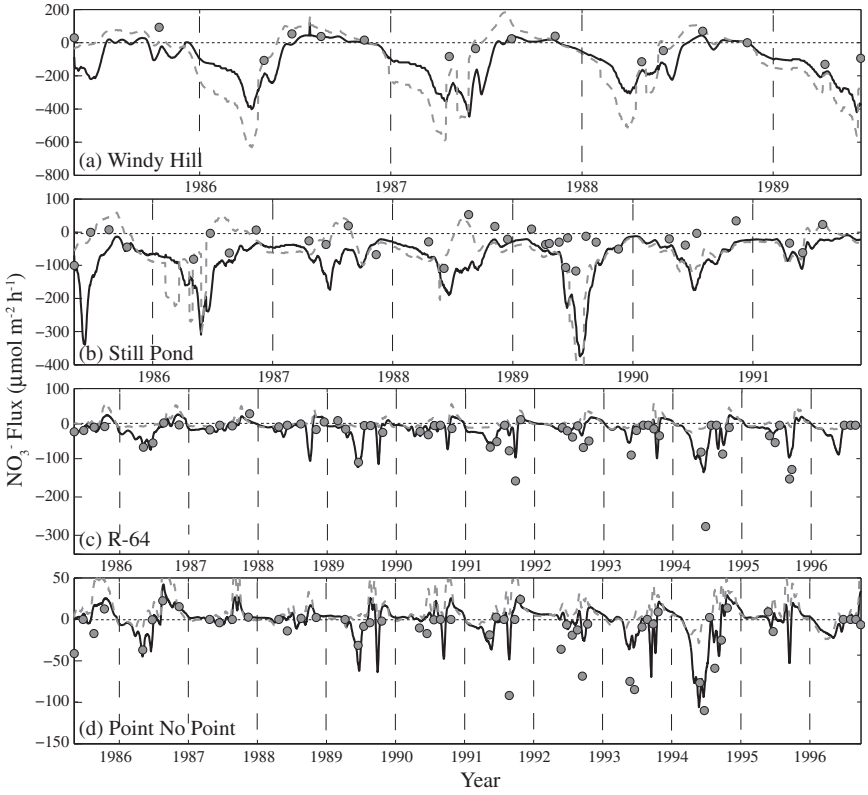

Fig. 6. Modeled (lines) and observed (circles) time series of NO_3^- flux from four stations in Chesapeake Bay (a: Windy Hill, b: Still Pond, c: R-64, d: Point No Point). Gray dashed lines represent model output using a layer 1 denitrification velocity of 0.1 m day^{-1} from the original calibration, while black solid lines represent model output using the depth-independent, aerobic-layer denitrification model of 0.2 m day^{-1}.

3.2. Denitrification

In addition to model-data comparisons of NO_3^- fluxes, it was also possible to validate model-computed denitrification rates (using the depth-independent formulation) with observations made at several stations within Chesapeake Bay (Fig. 7). Denitrification has been measured across a wide range of conditions (i.e., overlying-water NO_3^-, salinity, O_2, and depth) in Chesapeake Bay over the past several decades (Kemp et al., 1990; Kana et al., 1998) using a variety of methods. A collection of measurements made in the Choptank River estuary over a large gradient (3–300 μM) of overlying-water NO_3^- (Kana et al., 1998) demonstrated a strong dependence of denitrification on NO_3^- availability in the overlying water (Piña-Ochoa and Álvarez-Cobelas, 2006). When seasonally-averaged, modeled denitrification rates for each station are plotted against overlying-water NO_3^-, the overall relationship and rate magnitudes compare favorably to observations (Fig. 7a).

At stations R-64 and Still Pond, denitrification rates estimated over an annual cycle in 2000 and 2001 match the seasonality and magnitude of SFM predictions (Fig. 7b and c). In general, two different seasonal patterns of denitrification were predicted by SFM for two distinct environmental types; at stations with high NO_3^- and no seasonal hypoxia, denitrification followed the annual temperature cycle (e.g., Still Pond), whereas stations with low summer NO_3^- and seasonal hypoxia or anoxia, denitrification displayed a bimodal cycle (e.g., R-64; Fig. 7b).

3.3. Phosphate flux

Unlike NO_3^-, the original model calibration resulted in sediment-water PO_4^{3-} fluxes that agreed with the data reasonably well (Fig. 8, Table 4), as evidenced by a reliability index of 1.41 (well below 2). However, model estimates of PO_4^{3-} fluxes were particularly high during the summer at anoxic stations compared with observed fluxes (Fig. 8b). Optimization routines suggested station-specific values for the aerobic ($\Delta\pi_{PO_4^{3-},1}$) and anaerobic ($\pi_{PO_4^{3-},2}$) layer partition coefficients significantly improved model fit during this important seasonal period of internal phosphorus loading. Model-observation fits resulted in an overall RMSE reduction of 25% when $\Delta\pi_{PO_4^{3-},1}$ and $\pi_{PO_4^{3-},2}$ were higher at low salinity sites in close proximity to river inputs (Still Pond, Maryland Point; Fig. 8c, Table 4) and when $\Delta\pi_{PO_4^{3-},1}$ and $\pi_{PO_4^{3-},2}$ were lower at most other sites (Fig. 8c, Table 4). In some cases (e.g., R-78, Point No Point), the model was insensitive to changes in the partitioning coefficients. Station-specific values of $\Delta\pi_{PO_4^{3-},1}$ were related to the amount of oxalate-extractable Fe observed in the top 3 cm of sediments (Cornwell and Sampou, 1995) at four sites in Chesapeake Bay (Fig. 8c inset). Where Fe concentrations were higher, the aerobic layer partitioning coefficient optimized at higher values (Fig. 8c inset). When the optimized parameters were included in SFM simulations, the model better represented the observed sediment-water fluxes, particularly during summer (Fig. 9, Table 4). When the PO_4^{3-} flux was optimized to J_{PIP}, RMSE was slightly improved (Table 4), with J_{PIP} contributing between 25% and 50% of total phosphorus deposition (data now shown).

3.4. Nitrogen and phosphorus recycling

O_2 concentration exerts strong control over nitrogen and phosphorus cycling in sediments. To explore the role overlying water O_2 in the removal of nutrients by sediments, sediment-water fluxes of NH_4^+ and PO_4^{3-} were plotted against the deposition of

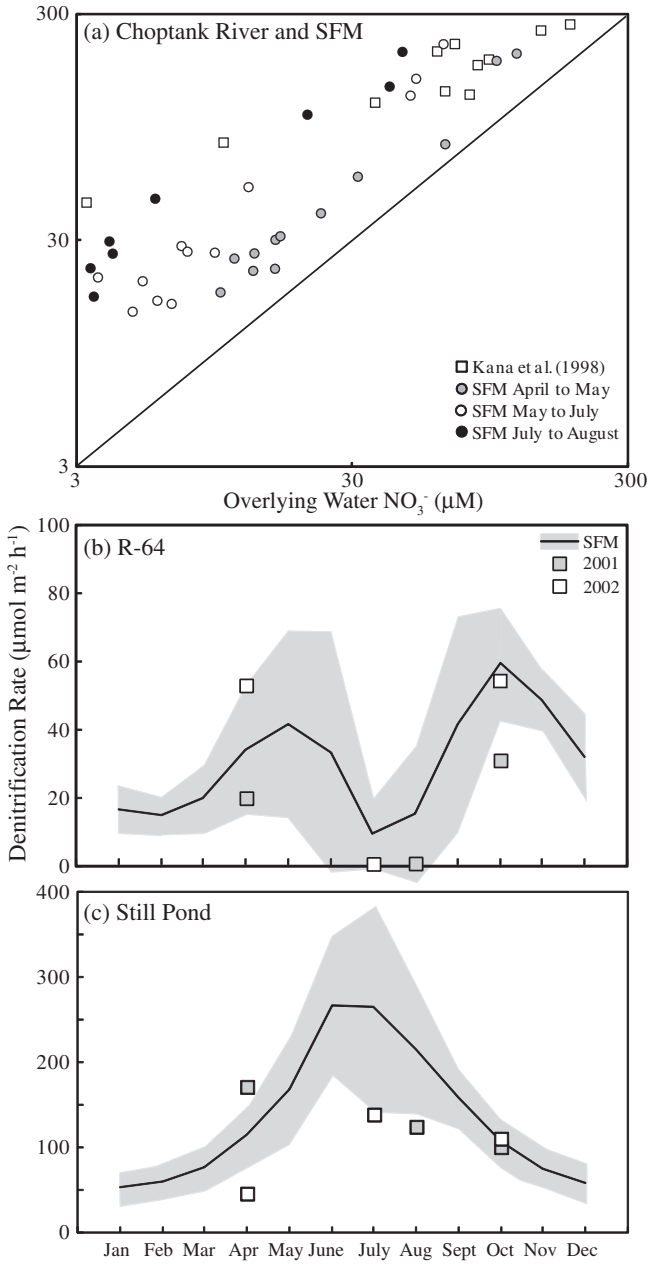

Fig. 7. (a) Relationship between overlying-water NO_3^- and sediment denitrification rates as observed (squares) in the Choptank River estuary (Kana et al., 1998) and modeled for all stations over 3 seasons with SFM (circles). (b) Seasonal cycle of modeled (line is mean, shaded area is ±1SD) and observed (squares) sediment denitrification at R-64 and (c) Still Pond.

organic N and P (Fig. 10). Between 25% and 50% of the deposited nitrogen was removed (via burial or denitrification), while in general, 25% of the phosphorus was removed (via burial or storage). Nitrogen removal was higher at stations where summer O_2 concentrations generally do not become anoxic (Fig. 10). At Still Pond and Maryland Point, where O_2 concentrations are above 95 µM year-round and partitioning coefficients (i.e., Fe concentrations) are high (Fig. 10), phosphorus removal was >50%. Another method of assessing O_2 effects on nitrogen cycling is to compute the "nitrogen recycling efficiency" $\left(NRE = \frac{J[NH_4^+]}{J[NH_4^+]+J[N_2]+J[NO_3^-]}\right)$ from the model nitrogen fluxes (Boynton and Kemp, 2008), which represents NH_4^+ recycling relative to the total efflux of inorganic N solutes. This index, computed from model simulations, was negatively correlated to overlying water O_2 concentrations at all sites in Chesapeake Bay ($r > 0.95$, $p < 0.001$; Fig. 10, inset).

3.5. Dissolved silica flux

The original calibration of the silica model generally resulted in an underestimation of the sediment-water DSi flux, especially during warmer months (Fig. 11). SFM originally considered silica solubility to be constant in time. However, when SFM was run at all stations with silica solubility formulated as an exponential function of temperature $Si_{sat} = Si_{sat,20}\theta_{Si}^{(T-20)}$ (Lawson et al., 1978), the model improved slightly (Table 4). Optimizations indicated that the model was insensitive to changes in $K_{M,PSi}$ and k_{Si} (data not shown), where values were applicable to all Chesapeake Bay stations. Optimization routines suggested that the inorganic (i.e., non-biogenic) silica deposition rate ($J_{Detr_{Si}}$) of 1.8 mmol Si m^{-2} d^{-1} was 22%–46% of biogenic silica fluxes at all stations except R-78 (where it was 67%).

SFM includes an O_2-dependent sorption of DSi onto particles (partitioning), which represents DSi binding onto FeOOH under oxygenated conditions (as with PO_4^{3-}). The anaerobic-layer partition coefficient, $\pi_{Si,2}$, was similar to PO_4^{3-} in the original calibration, yet there is a limited literature to suggest strong binding of DSi to FeOOH under the conditions found in most estuarine sediments. Thus, we optimized the model for $\Delta\pi_{Si,1}$ and $\pi_{Si,2}$, and found that RMSE, ME, and RI of DSi flux were uniformly reduced across all stations when the partition coefficients were reduced from 10 to 5 ($\Delta\pi_{Si,1}$) and from 100 to 15 ($\pi_{Si,2}$) at the anoxic sites (Table 4), with a 36% reduction in RMSE across sites. The optimized values or $\Delta\pi_{Si,1}$ (15) and $\pi_{Si,2}$ (50) were higher at the oxic, low-salinity sites (Still Pond, Maryland Point; Tables 2 and 4). The resulting seasonal pattern of DSi more closely fit that of the observations (Fig. 11).

4. Discussion

This paper illustrates the simulation skill and flexibility of application for the stand-alone version of SFM with a focus on analyzing sediment-water fluxes of NH_4^+, NO_3^-, N_2, PO_4^{3-}, and DSi. Here we have demonstrated a range of ways that the model can complement field measurements to estimate unmeasured processes and simulate inter-annual variations in biogeochemical processes.

4.1. Nitrogen cycling

After model reformulation and parameter optimization, SFM simulated NO_3^- fluxes that agreed well with observations across many stations with varying salinity, O_2, and organic matter deposition rates. The same is true for NH_4^+ fluxes, which are described in detail in a companion publication (Brady et al., 2013). For NO_3^- simulations, it was clear the original value of $\kappa_{NO_3^-,1}$ and the associated NO_3^- flux were underestimated for the majority of stations we tested in Chesapeake Bay. This "missing" NO_3^- uptake could result from an under-prediction of denitrification rates or a result of the fact that SFM does not include dissimilatory nitrate reduction to ammonium, or DNRA (Kelly-Gerreyn et al., 2001; An and Gardner, 2002). Because we lack sufficient information to model DNRA in Chesapeake Bay, but have access to denitrification measurements, we explored how under-estimated denitrification rates might be contributing to the "missing NO_3^- uptake. Optimized values for $\kappa_{NO_3^-,1}$ were inversely correlated to the depth of the aerobic layer across the stations in our analysis; that is, where the aerobic layer

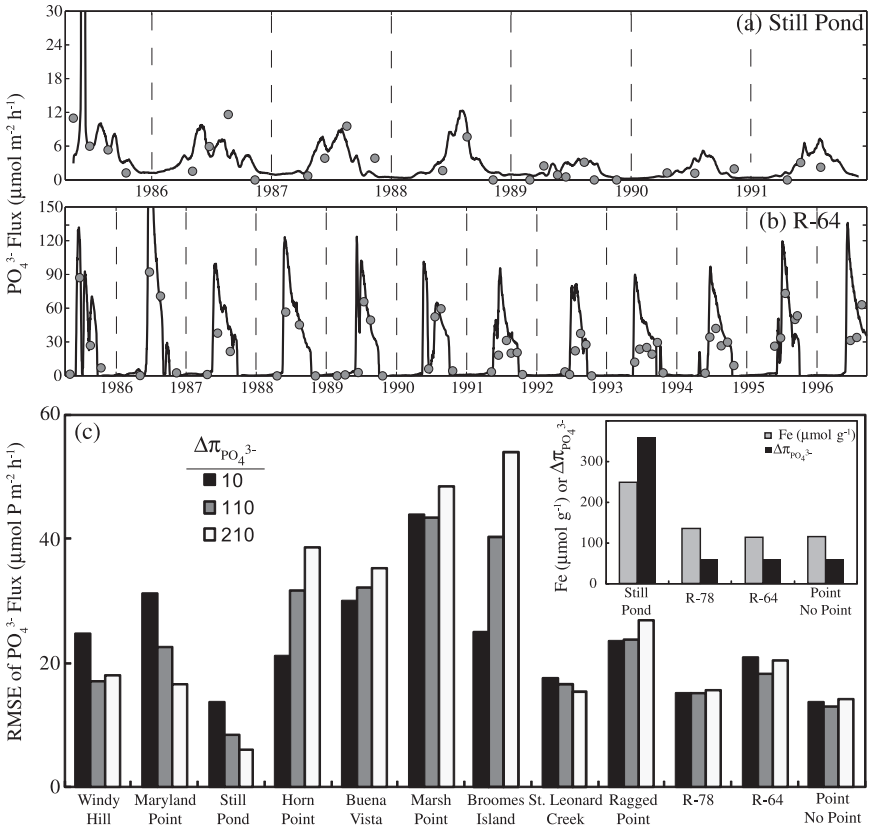

Fig. 8. Modeled (lines) versus observed (circles) sediment-water PO_4^{3-} flux at Still Pond (a) and R-64 (b), where model computations were made using an aerobic-layer partitioning coefficient of 300 kg l^{-1} from the original calibration. (c) Comparison of RMSE values for modeled PO_4^{3-} flux across all stations at varying values of the aerobic-layer partitioning coefficient, where the optimized value for $\Delta\pi PO_4^{3-}$, 1 is highly correlated to observed oxalate-extractable Fe (inset) in the top 10 cm of sediments (Cornwell and Sampou, 1995).

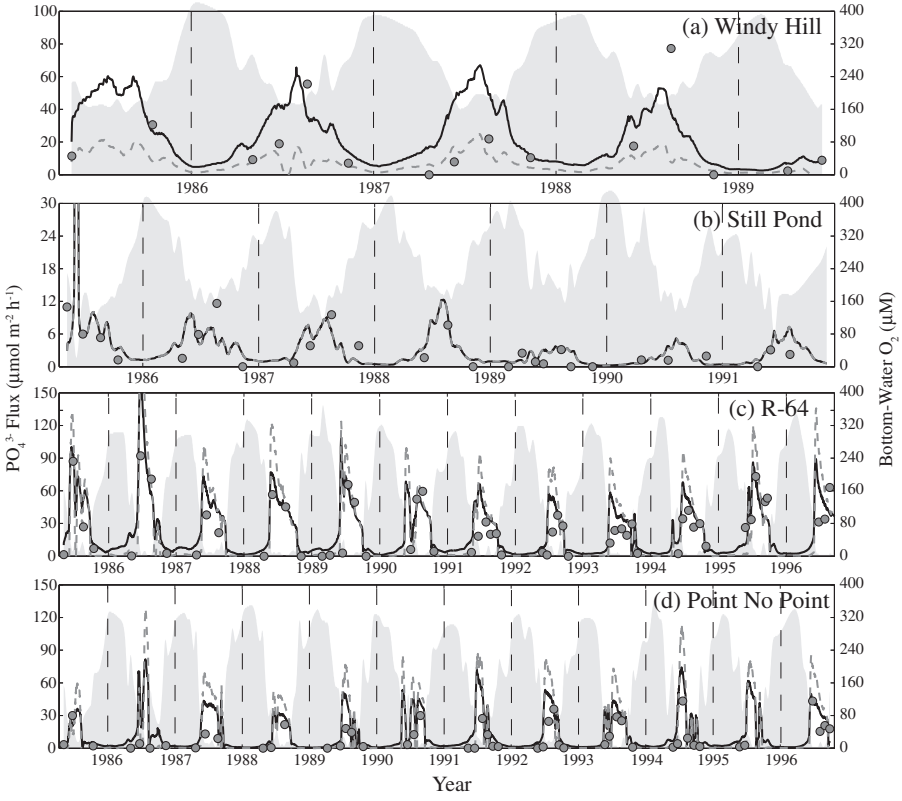

Fig. 9. Modeled (lines) and observed (circles) time series of PO_4^{3-} flux from four stations in Chesapeake Bay (a: Windy Hill, b: Still Pond, c: R-64, d: Point No Point). Gray dashed lines represent model output using the original aerobic-layer partition coefficient ($\Delta\pi PO_4^{3-}$, 1) and black solid lines represent the station-specific optimized $\Delta\pi PO_4^{3-}$, 1. Grey areas are overlying-water O_2 concentrations at each station during the simulation.

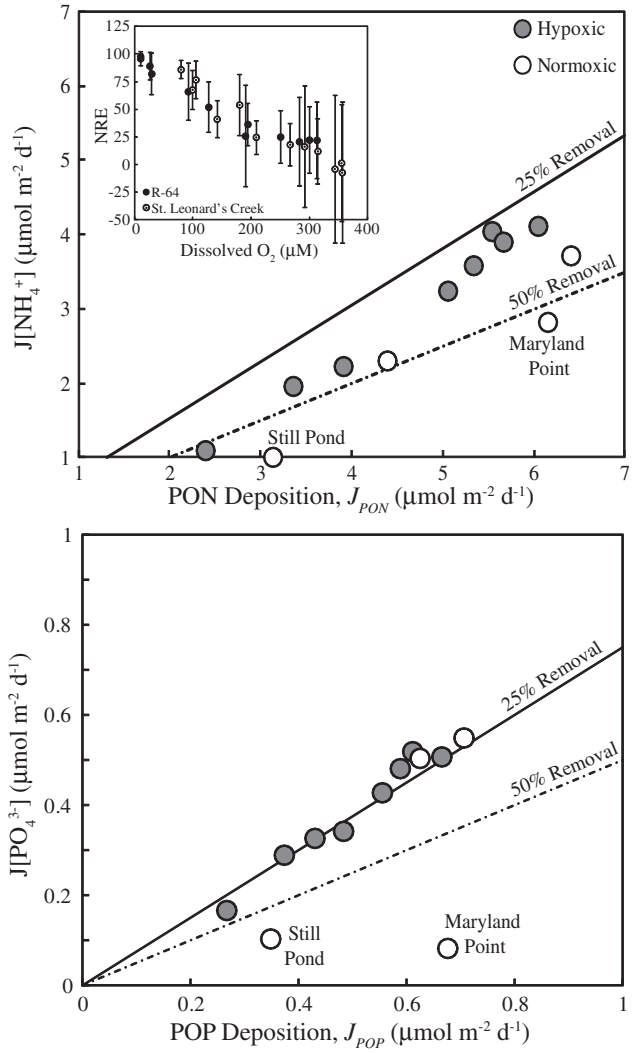

Fig. 10. Relationship of modeled sediment-water NH_4^+ (top panel) and PO_4^{3-} (bottom panel) fluxes to PON and POP deposition, respectively, at each station in Chesapeake Bay. Open circles are stations characterized by oxygenated conditions throughout the year in the overlying-water, which shaded circles represent stations with seasonal hypoxia or anoxia. Data are means over the model period, which is specific to each station. Lines represent the percentage of N or P removed (via denitrification, burial, or long-term storage) from that deposited. The inset figure is the relationship of "Nitrogen Recycling Efficiency" ($NRE = J[NH_4^+]/J[NH_4^+] + J[N_2] + J[NO_3^-]$) to overlying water O_2 at R-64 and St. Leonard's Creek, where data are monthly means.

depth was large, $\kappa_{NO_3^-,1}$ was low. Because SFM assumes that denitrification is occurring uniformly throughout each layer, the NO_3^- loss rate associated with denitrification will be larger for a given value of $\kappa_{NO_3^-,1}$ as the aerobic layer depth increases. Thus, we removed the depth-dependence from the aerobic-layer denitrification formulation.

Although denitrification is considered to be a strictly anaerobic process, evidence exists for denitrification within the aerobic zone associated with "anoxic microsites" in organic aggregates (Jørgensen, 1977; Jenkins and Kemp, 1984). The inclusion of aerobic-layer denitrification in SFM, although absent from conventional sediment diagenesis models (Vanderborght et al., 1977b; Jahnke et al., 1982), has been included in more recent work (Brandes and Devol, 1995). If the aerobic-layer denitrification is occurring in anoxic microsites, we have no reason to assume that these sites would not be equally distributed. Denitrification may be active in sections of sediments where there is close spatial coupling between the anoxic zone and the high-NO_3^- zone, which is nearly always aerobic (Blackburn et al., 1994). If this was the case, modeled denitrification would only occur in a relatively thin section of the sediment at the interface of the aerobic and anaerobic layer, and thus the denitrification loss term in SFM should be depth-independent. We applied such a formulation in SFM and found good model-data agreement across sites at a single value for the aerobic layer denitrification rate (Fig. 6, Table 4). It should be noted that sediment models that resolve porewater profiles with high vertical resolution do not need such a formulation, as interfaces within strong, opposing concentration gradients are well-represented.

Modeled denitrification rates agreed well with observations (Kana et al., 1998) and indicate the potential to model seasonal cycles of an important process that is effort intensive to measure (Fig. 7). Measurements of sediment denitrification were found to be strongly tied to overlying-water NO_3^- in the Choptank River (Kana et al., 1998), as well as many other locations (Seitzinger et al., 1993; Pelegrí and Blackburn, 1995; Dong et al., 2000). SFM simulations fit this pattern across all sites in Chesapeake Bay and during three seasons (Fig. 7a). The intercept of a linear model fit of overlying-water NO_3^- and denitrification rates indicates the degree of nitrification (Kana et al., 1998). We compared this intercept (as derived for each station and month) to SFM-modeled nitrification rates and found that the intercept value was highly correlated ($r > 0.8$) with the modeled rates (Di Toro, 2001). From a seasonal perspective, denitrification appears to have two maxima at seasonally-hypoxic stations (Fig. 7b), one in April–June and another in October–November (Kemp et al., 1990). This has been observed in other systems as well (Jørgensen and Sørensen, 1988) and primarily results from NO_3^- limitation during periods of the year (i.e., summer) when sediment nitrification is limited by low O_2 and high sulfide concentrations (Henriksen and Kemp, 1988). Conversely, at stations with ample NO_3^- concentrations in overlying water year-round (e.g., Maryland Point, Still Pond), high denitrification rates were maintained throughout summer and followed the annual temperature cycle (Fig. 7c).

Previous studies have used cross-system comparisons to estimate the fraction of external nitrogen loading that is lost to the atmosphere via denitrification as roughly 50% (Seitzinger, 1988). An analysis of SFM data indicated that between 50% and 75% of the PON flux to sediments was released as NH_4^+ (Fig. 10), indicating that 25%–50% of the depositional flux was either lost to the atmosphere via coupled nitrification-denitrification or it was buried in sediments. For the majority of sites in Chesapeake Bay, denitrification on average accounted for 25% of the PON flux, while burial of PON has been reported to be 15%–25% of PON deposition (Kemp et al., 1990; Boynton et al., 1995). Interestingly, the $J[NH_4^+]/J_{PON}$ ratio was higher at 8 of the 12 stations we modeled that experienced seasonal hypoxia or anoxia relative to those that did not; this indicates that hypoxia-driven summertime declines in denitrification resulted in a larger fraction of J_{PON} being released as NH_4^+ (Fig. 10) as has been observed previously in many other coastal ecosystems (Seitzinger and Nixon, 1985; Kemp et al., 1990).

Recent research has indicated that previously underappreciated aspects of the nitrogen cycle maybe be important in marine ecosystems (Burgin and Hamilton, 2007). These include, but are not limited to, dissimilarity reduction of nitrate to ammonium (DNRA), anaerobic ammonium oxidation (anammox), and nitrogen fixation associated with sulfate reduction (Bertics et al., 2010; Brunet and Garcia-Gill, 1996; Dalsgaard and Thamdrup, 2002; Gardner et al., 2006; Rich et al., 2008). SFM does not include these processes, primarily because we do not yet have the data to support model formulation and validation of these

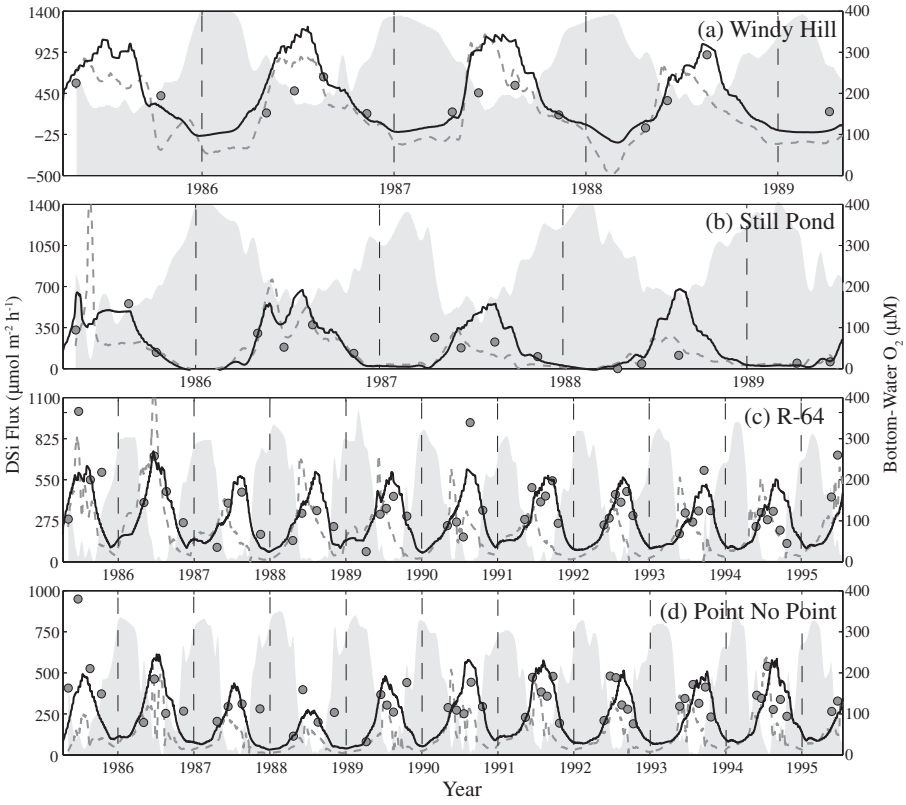

Fig. 11. Modeled (lines) and observed (circles) time series of DSi flux from four stations in Chesapeake Bay (a: Windy Hill, b: Still Pond, c: R-64, d: Point No Point). Gray dashed lines represent model output using the original calibration, while black solid lines represent simulations with modeled temperature-dependent Si_{sat}, optimized parameters (see text), and station-specific optimized $\Delta\pi_{Si,1}$ and $\Delta\pi_{Si,2}$.

processes, especially in Chesapeake Bay. Some of these processes may be indirectly modeled; for example, N_2 production due to anammox may be "parameterized" in the modeled denitrification. It is clear from our experience here that future modeling studies may add equations and parameters to simulate these processes explicitly as more information on controlling processes becomes available.

Despite the reasonable model performance with respect to NO_3^- flux (Table 4), it is clear that in some years, the model over-estimated NO_3^- influxes at some stations (Windy Hill, Still Pond), but under-estimated influxes at others (R-64, Pint No Point, Fig. 6). At shallow, oxic stations (e.g., Still Pond), these high NO_3^- influxes were the result of slightly over-estimated denitrification rates (Figs. 6 and 7). The reasons why NO_3^- influxes were under-predicted at deeper, seasonally anoxic sites (e.g., R-64) were less clear. Considering that denitrification rates tended to agree with observations at these stations, it may be that DNRA was active and consuming NO_3^- in larger quantities than predicted, leading to larger sediment-water NO_3^- gradients and associated fluxes. However, NH_4^+ fluxes are accurately simulated at these stations (Brady et al., 2013), suggesting that any process that would generate additional NH_4^+ is not the cause of the discrepancy. Because porewater distributions of NO_3^- may be more complex than would be simulated with a two-layer model (Vanderborght et al., 1977b; Soetaert et al., 1996b), the discrepancies could simply illustrate a limitation of the simplified model domain.

4.2. Phosphorus cycling

SFM-simulated PO_4^{3-} fluxes agreed well with observations across many stations, but the comparisons were slightly more complex due to solute–particle interactions. The adsorption of PO_4^{3-} onto FeOOH (as well as manganese oxides) is an important mechanism of temporary phosphorus storage in marine sediments (Sundby et al., 1992; Slomp et al., 1998), which can dominate dissolved PO_4^{3-} dynamics near the sediment-water interface (Krom and Berner, 1981) and control seasonal cycles of sediment-water PO_4^{3-} fluxes (Cowan and Boynton, 1996). Optimization routines indicated a spatial-dependence of the optimal aerobic-layer partitioning coefficients and the strong relationship between these coefficients and observed oxalate-extractable Fe availability illustrates elevated PO_4^{3-} sorption within Fe-rich sediments near the land–water interface (Upchruch et al., 1974; Spiteri et al., 2008). Lower PO_4^{3-} retention via sorption (i.e., lower partitioning coefficient) is also consistent with the removal of Fe via precipitation with sulfides in more saline regions of the estuary (Caraco et al., 1989; Jordan et al., 2008), although these dynamics are not specifically modeled in SFM. Although the incorporation of site-specific parameters into models is not ideal, we justify spatially-varying partition coefficients because Fe is not modeled explicitly and because partition coefficients could potentially be predicted from known Fe concentrations.

Although many previous models of PO_4^{3-} have emphasized diagenetic production and the resultant vertical porewater profiles (Van Cappellen and Berner, 1988; Rabouille and Gaillard, 1991), other models have examined the influence of PO_4^{3-} sorption and desorption on the availability and sediment-water fluxes (Slomp et al., 1998; Wang et al., 2003). The evolution of seasonal increases in sediment-water PO_4^{3-} fluxes in Chesapeake Bay often lags by a month or more after NH_4^+ increases (Cowan and Boynton, 1996). This phenomenon has been explained by the adsorption of diagenetically-produced PO_4^{3-} to FeOOH in the aerobic layer under

oxic conditions, which buffers porewaters and results in low concentrations and sediment-water fluxes. Similar interactions do not limit NH_4^+ sediment-water fluxes, thus diagenetically-produced NH_4^+ is free to diffuse to the overlying water. Under reduced oxygen conditions characteristic of several regions of Chesapeake Bay, iron is reduced, thereby releasing the stored PO_4^{3-} to the water column later in summer (Testa and Kemp, 2012). The use of oxygen-dependent partitioning coefficients allows for the representation of these processes; when such coefficients are removed, the annual PO_4^{3-} flux cycle closely resembles that of NH_4^+ (data not shown). Because the partitioning coefficients are sensitive to O_2, the model suggests large PO_4^{3-} effluxes when O_2 is first depleted in late spring (Fig. 9). Although these large effluxes are not always reflected by the observations, this may simply be a result of the observations being too sparse to capture these short-lived events. Because this formulation otherwise represents an instantaneous partitioning between solid and dissolved PO_4^{3-}, where other formulations consider different adsorption rates as a function of the crystalline structure of the FeOOH (Slomp et al., 1998), a more detailed formulation in SFM may improve model-data agreement. We lack the data necessary to represent such detailed FeOOH structure in the model.

An analysis of SFM data indicated that roughly 75% of the POP flux to sediments was released as PO_4^{3-} (Fig. 10), indicating that 25% of the depositional flux was either buried or stored in the active sediment. The $J[PO_4^{3-}]/J_{POP}$ ratio was lower at 2 of the 12 stations we modeled and these two stations were where partitioning coefficients were higher and overlying-water O_2 concentrations remained above 100 μM year-round. This indicates that burial processes are similar across sites and that relatively high O_2 can maintain PO_4^{3-} in sediments.

4.3. Silica cycling

The calibration process for the silica sub-model in SFM resulted in simulated DSi fluxes that agreed well with observations across many stations and provided insights on key processes affecting sediment silica biogeochemistry. First, the addition of a temperature-dependent silica solubility formulation is consistent with experimental work (Lawson et al., 1978; Van Cappellen and Linqing, 1997a) and removed the constraint on porewater DSi accumulation imposed by the fixed solubility (900 mM) in the original model. In turn, model porewater DSi concentrations increased in warmer periods to generate the sediment-water concentration gradient necessary to better match observed DSi fluxes (Fanning and Pilson, 1974; Schink et al., 1974). Such controls contribute to the strong temperature-dependency on sediment-water DSi fluxes in Chesapeake Bay (Yamada and D'Elia, 1984).

Porewater DSi accumulation is also strongly dependent on the dissolution rate constant (k_{Si}), but reported values of this parameter vary between 10^{-7} and 10^{-9} s^{-1} (Vanderborght et al., 1977a; Wong and Grosch, 1978; Rabouille and Gaillard, 1990). Such variation is due to differences in the diatom species being dissolved, the residence time of the algal cells in the water column prior to deposition, alterations of the siliceous material within the sediment (Schink et al., 1975; Rabouille and Gaillard, 1990), and other factors. Considering the temperature dependence for this first-order reaction constant in SFM, the optimized value for k_{Si} in SFM varies from 4.3×10^{-7} to 7.5×10^{-6} over the course of the year, which is somewhat faster than other values reported in the literature during warm months (Table 3). However, SFM considers the deposition of relatively fresh organic matter, which may explain the faster dissolution rates compared to natural samples of diverse siliceous material from less productive regions (Schink et al., 1975). The faster dissolution rate may also represent enhanced silica dissolution due to bacterial activity (Bidle and Azam, 1999), which is generally high in productive, eutrophic estuaries.

The major improvement to the silica model in SFM, however, resulted from reducing the solid-solute partitioning coefficients that represent the sorption/desorption of DSi with FeOOH. O_2-dependent partitioning allows for the storage of diagenetically-produced PO_4^{3-} and DSi in sediments until low O_2 conditions lead to FeOOH dissolution and PO_4^{3-}/DSi release. Although sorption dynamics between PO_4^{3-} and FeOOH are well-described (Sundby et al., 1992), silica is less affected by these interactions than PO_4^{3-} (Mayer and Gloss, 1980) and DSi fluxes have been found to be relatively insensitive to O_2 (Yamada and D'Elia, 1984). Indeed, most sediment silica models do not include sorption of DSi to FeOOH (Schink et al., 1975; Wong and Grosch, 1978). When we reduced the partitioning coefficients at all sites, the model representation of DSi fluxes improved substantially, with a more representative seasonal cycle (Fig. 11). With the partitioning formulation active, SFM predicts large and short-lived peaks in DSi flux in late spring at stations where O_2 reaches anoxic and hypoxic levels (e.g., R-64, Point No Point). This is due to temporary storage of DSi sorbed to FeOOH during spring followed by abrupt and large sediment-water effluxes of DSi when O_2 declines below 62.5 μM (data not shown). With the removal of this temporary storage mechanism for SFM, DSi is stored in lower quantities during spring and is released gradually through summer as it dissolves, and the resulting fluxes better match observations (Fig. 11, Table 4). Despite this improvement, the model does not capture some dynamics of the DSi flux in certain years. This may be a result of uncertainty in seasonal and interannual variations in particulate silica deposition to sediments, which vary as a function of freshwater input (Conley and Malone, 1992), the dominant phytoplankton species (Parsons et al., 1961), as well as other controls on dissolution (Michalopoulos and Aller, 2004).

4.4. Model improvements

There are some limitations of the SFM sub-models described here that could be improved in the future. Although SFM's two-layer vertical resolution limits its ability to simulate fine scale, vertically distinct processes, its simplicity adds to the model's flexibility as a linked component in 3D biophysical models and as a tool in stand-alone applications (Vanderborght et al., 1977a, b). SFM now includes a benthic algal sub-module (Cerco and Setzinger, 1997) that considers the interactions between benthic algae and sediment-water fluxes. This addition allows the use of SFM in shallow-water ecosystems where light reaches the sediments. Although the denitrification formulations in SFM originally lacked a limitation by organic carbon (Di Toro, 2001), we have added this dependency to SFM, thereby improving its applicability in more carbon-limited systems. We related the regional-specificity in the optimized phosphorus partition coefficients to the concentration (and thus availability of sorption sites) of FeOOH. A more mechanistic alternative is to explicitly model iron (e.g., Wang and Van Cappellen, 1996; Reed et al., 2011); an iron model has been developed within the SFM framework (Chapter 21 in Di Toro, 2001) and could be integrated with the nutrient and O_2 sub-modules of SFM in the future. The parameter optimization scheme described here allows for relatively fast (i.e., less than 1 h) sensitivity tests and parameter adjustment for applications in new systems is straightforward. Finally, an explicit representation of aerobic respiration could be included, as well as recently emphasized pathways within the nitrogen cycle, such as DNRA and anammox.

An important goal in the calibration and development of any model is the balance between generality, realism, and precision (Levins, 1966). Because SFM is ideally applicable to a wide-variety of ecosystems, it occasionally became necessary to sacrifice precision

in any one environment to develop a more general set of equations to represent a given suite of key processes (e.g., Imteaz et al., 2003). Beyond these key processes, there are many reactions we know exist in reality, but to date have not been sufficiently studied and cannot be meaningfully represented in a model. Thus, although all models necessarily simplify a complex-ecosystem into a set of mathematical formulations that can practically represent system behavior, it is advantageous to develop general models with the flexibility to add realism as the state-of-the-science progresses. Although calibration exercises can result in parameter sets that enhance model precision while sacrificing generality (as in this study), ultimately some level of human judgment must be involved in evaluating trade-offs (Cerco and Noel, 2005) and exploring the potential to gain biogeochemical insight from the modeling process.

Acknowledgments

We would like to thank James Fitzpatrick for the many discussions we have had related to topics covered in this manuscript. We would also like to thank the United States Environmental Protection Agency Chesapeake Bay Program and the Maryland Department of Natural Resources for collecting many of the data presented in this work. Partial funding for our contribution to this work came from the United States National Oceanographic and Atmospheric Administration (NOAA) Coastal Hypoxia Research Program (CHRP-NAO7-NOS4780191), the National Science Foundation (Chesapeake Bay Environmental Observatory; CBEO-3 BERS-0618986 and Biocomplexity Research; OCE-9981617), and by the State of Maryland Department of Natural Resources (K00B920002). This work is NOAA Coastal Hypoxia Research Program (CHRP) Publication # 182 and the University of Maryland Center for Environmental Science Contribution # 4771. This research was also partially funded by the U.S. Water Environment Research Federation under Grant No. U4R09.

References

Abdollahi, H., Nedwell, D.B., 1979. Seasonal temperature as a factor influencing bacterial sulfate reduction in a saltmarsh sediment. Microbial Ecology 5, 73–79.

An, S., Gardner, W.S., 2002. Dissimilatory nitrate reduction to ammonium (DNRA) as a nitrogen link, versus denitrification as a sink in a shallow estuary (Laguna Madre/Baffin Bay, Texas). Marine Ecology Progress Series 237, 41–50.

Antoniou, P., Hamilton, J., Koopman, B., Jain, R., Holloway, B., Lyberatos, G., Svoronos, S.A., 1990. Effect of temperature and pH on the effective maximum specific growth rate of nitrifying bacteria. Water Research 24, 97–101.

Argaman, Y., Miller, E., 1979. Modeling recycled systems for biological nitrification and denitrification. Journal of Water Pollution Control Federation, 749–758.

Baden, S.P., Loo, L.O., Pihl, L., Rosenberg, R., 1990. Effects of eutrophication on benthic communities including fish: Swedish west coast. Ambio 19, 113–122.

Balzer, W., 1996. Particle mixing processes of Chernobyl fallout in deep Norwegian Sea sediments: evidence for seasonal effects. Geochimica et Cosmochimica Acta 60, 3425–3433.

Beauchard, O., Ciutat, A., Gerino, M., Munoz, T., Jacobs, S., Tackx, M., Stora, G., Meire, P., 2012. Spatiotemporal bioturbation patterns in a tidal freshwater marsh. Estuarine, Coastal and Shelf Science 96, 159–169.

Bertics, V.J., Sohm, J.A., Treude, T., Chow, C.E.T., Capone, D.C., Fuhrman, J.A., Ziebis, W., 2010. Burrowing deeper into benthic nitrogen cycling: the impact of bioturbation on nitrogen fixation coupled to sulfate reduction. Marine Ecology Progress Series 409, 1–15.

Bertics, V.J., Löscher, C.R., Salonen, I., Dale, A.W., Gier, J., Schmitz, R.A., Treude, T., 2013. Occurrence of benthic microbial nitrogen fixation coupled to sulfate reduction in the seasonally hypoxic Eckernförde Bay, Baltic Sea. Biogeosciences 10, 1243–1258.

Bidle, K.D., Azam, F., 1999. Accelerated dissolution of diatom silica by marine bacterial assemblages. Nature 397, 508–512.

Billen, G., 1982. An idealized model of nitrogen recycling in marine sediments. Journal of American Science 282, 512–541.

Blackburn, T.H., Blackburn, N.D., Jensen, K., Risgaard-Petersen, N., 1994. Simulation model of the coupling between nitrification and denitrification in a freshwater sediment. Applied and Environmental Microbiology 60, 3089–3095.

Boudreau, B.P., 1991. Modelling the sulfide-oxygen reaction and associated pH gradients in porewaters. Geochimica et Cosmochimica Acta 55, 145–159.

Boynton, W.R., Bailey, E., 2008. Sediment Oxygen and Nutrient Exchange Measurements from Chesapeake Bay, Tributary Rivers and Maryland Coastal Bays: Development of a Comprehensive Database and Analysis Factors Controlling Patterns and Magnitude of Sediment-water Exchanges. University of Maryland Center for Environmental Science, Solomons, MD, p. 202.

Boynton, W.R., Kemp, W.M., 2008. Estuaries. In: Capone, D.G., Bronk, D.A., Mulholland, M.R., Carpenter, E.J. (Eds.), Nitrogen in the Marine Environment, second ed. Elsevier, Amsterdam, pp. 809–866.

Boynton, W.R., Garber, J.H., Summers, R., Kemp, W.M., 1995. Inputs, transformations, and transport of nitrogen and phosphorus in Chesapeake Bay and selected tributaries. Estuaries 18, 285–314.

Brady, D.C., Testa, J.M., Toro, D.M.D., Boynton, W.R., Kemp, W.M., 2013. Sediment flux modeling: calibration and application for coastal systems. Estuarine, Coastal and Shelf Science 117, 107–124.

Brandes, J.A., Devol, A.H., 1995. Simultaneous nitrate and oxygen respiration in coastal sediments: evidence for discrete diagenesis. Journal of Marine Research 53, 771–797.

Brunet, R.D., Garcia-Gill, L.J., 1996. Sulfide-induced dissimilatory nitrate reduction to ammonia in anaerobic freshwater sediments. FEMS Microbiology Letters 21, 131–138.

Burdige, D.J., 1991. The kinetics of organic matter mineralization in anoxic marine sediments. Journal of Marine Research 49, 727–761.

Burgin, A.J., Hamilton, S.K., 2007. Have we overemphasized the role of denitrification in aquatic ecosystems? A review of nitrate removal pathways. Frontiers in Ecology and the Environment 5, 89–96.

Cai, W.-J., Sayles, F.L., 1996. Oxygen penetration depths and fluxes in marine sediments. Marine Chemistry 52, 123–131.

Cai, W.-J., Luther III, G.W., Cornwell, J.C., Giblin, A.E., 2010. Carbon cycling and the coupling between proton and electron transfer reactions in aquatic sediments in Lake Champlain. Aquatic Geochemistry 16, 421–446.

Caraco, N.F., Cole, J.J., Likens, G.E., 1989. Evidence for sulphate-controlled phosphorus release from sediments of aquatic systems. Nature 341, 316–318.

Cerco, C.F., Cole, T., 1993. Three-dimensional eutrophication model of Chesapeake Bay. Journal of Environmental Engineering (ASCE) 119, 1006–1025.

Cerco, C.F., Noel, M.R., 2005. Incremental improvements in Chesapeake Bay environmental package. Journal of Environmental Engineering 131, 745–754.

Cerco, C.F., Setzinger, S.P., 1997. Measured and modeled effects of benthic algae on eutrophication in Indian River-Rehoboth Bay, Delaware. Estuaries 20, 231–248.

Conley, D.J., Malone, T.C., 1992. Annual cycle of dissolved silicate in Chesapeake Bay: implications for the production and fate of phytoplankton biomass. Marine Ecology Progress Series 81, 121–128.

Conley, D.J., Schelske, C.L., 1989. Processes Controlling the Benthic Regeneration and Sedimentary Accumulation of Biogenic Silica in Lake Michigan. Archiv fur Hydrobiologie, Stuttgart 116, pp. 23–43.

Conley, D.J., Schelske, C.L., Dempsey, B.G., Campbell, C.D., Newberry, T.L., 1986. Distribution of biogenic silica in the surficial sediments of Lake Michigan. CaJES 23, 1442–1449.

Conley, D.J., Schelske, C.L., Stoermer, E.F., 1993. Modification of the biogeochemical cycle of silica with eutrophication. Marine Ecology Progress Series 101, 179–192.

Conley, D.J., Humborg, C., Rahm, L., Savchuk, O.P., Wulff, F., 2002. Hypoxia in the Baltic Sea and basin-scale changes in phosphorus biogeochemistry. Environmental Science and Technology 36, 5315–5320.

Cooke, J.G., White, R.E., 1988. Nitrate enhancement of nitrification depth in sediment/water microcosms. Environmental Geology and Water Sciences 11, 85–94.

Cornwell, J.C., Sampou, P.A., 1995. Environmental controls on iron sulfide mineral formation in a coastal plain estuary. In: Vairamurthy, M.A., Schoonen, M.A.A. (Eds.), Geochemical Transformations of Sedimentary Sulfur. American Chemical Society, Washington D.C., pp. 224–242.

Cowan, J.L., Boynton, W.R., 1996. Sediment-water oxygen and nutrient exchanges along the longitudinal axis of Chesapeake Bay: seasonal patterns, controlling factors and ecological significance. Estuaries 19, 562–580.

Cowan, J.L., Pennock, J.R., Boynton, W.R., 1996. Seasonal and interannual patterns of sediment-water nutrient and oxygen fluxes in Mobile Bay, Alabama (USA): regulating factors and ecological significance. Marine Ecology Progress Series 141, 229–245.

Dalsgaard, T., Thamdrup, B., 2002. Factors controlling anaerobic ammonium oxidation with nitrite in marine sediments. Applied and Environmental Microbiology 6, 3802–3808.

Dhakar, S.P., Burdige, D.J., 1996. Coupled, non-linear, steady state model for early diagenetic processes in pelagic sediments. Journal of American Science 296, 296–330.

Di Toro, D.M., 2001. Sediment Flux Modeling. Wiley-Interscience, New York.

Di Toro, D.M., Fitzpatrick, J.J., 1993. Chesapeake Bay Sediment Flux Model. Chesapeake Bay Program Office, U.S. Environmental Protection Agency and U.S. Army Engineer District, Baltimore, Annapolis, Maryland and Baltimore, Maryland, p. 316.

Díaz, R.J., Rosenberg, R., 1995. Marine benthic hypoxia: a review of its ecological effects and the behavioural responses of benthic macrofauna. Oceanography and Marine Biology – An Annual Review 33, 245–303.

Dong, L.F., Thornton, D.C.O., Nedwell, D.B., Underwood, G.J.C., 2000. Denitrification in sediments of the River Colne estuary, England. Marine Ecology Progress Series 203, 109–122.

Emerson, S., Jahnke, R., Heggie, D., 1984. Sediment water exchange in shallow water estuarine sediments. Journal of Marine Systems 42, 709–730.
Fanning, K.A., Pilson, M.E.Q., 1974. The diffusion of dissolved silica out of deep-sea sediments. Journal of Geographical Research 79, 1293–1297.
Fennel, K., Wilkin, J., Levin, J., Moisan, J., O'Reilly, J., Haidvogel, D., 2006. Nitrogen cycling in the Middle Atlantic Bight: results from a three-dimensional model and implications for the North Atlantic nitrogen budget. Global Biogeochemical Cycles 20. http://dx.doi.org/10.1029/2005GB002456.
Gardner, W.S., McCarthy, M.J., An, S., Sobolev, D., Sell, K.S., Brock, D., 2006. Nitrogen fixation and dissimilatory nitrate reduction to ammonium (DNRA) support nitrogen dynamics in Texas estuaries. Limnology and Oceanography 51, 558–568.
Gee, C.S., Suidan, M.T., Pfeffer, J.T., 1990. Modeling of nitrification under substrate-inhibiting conditions. Journal of Environmental Engineering 116, 18–31.
Gerino, M., Aller, R.C., Lee, C., Cochran, J.K., Aller, J.Y., Green, M.A., Hirschberg, D., 1998. Comparison of different tracers and methods used to quantify bioturbation during a spring bloom: ^{234}thorium, luminophores and chlorophyll a. Estuarine, Coastal and Shelf Science 46, 531–547.
Goldhaber, M.B., Aller, R.C., Cochran, J.K., Rosenfeld, J.K., Martens, C.S., Berner, R.A., 1977. Sulfate reduction, diffusion, and bioturbation in Long Island Sound sediments; report of the FOAM Group. Journal of American Science 277, 193–237.
Grill, E.V., Richards, F.A., 1964. Nutrient regeneration from phytoplankton decomposing in seawater. Journal of Marine Research 22, 51–69.
Gypens, N., Lancelot, C., Soetaert, K., 2008. Simple parameterisations for describing N and P diagenetic processes: application in the North Sea. Progress in Oceanography 76, 89–110.
Heip, C.H.R., Goosen, N.K., Herman, P.M.J., Kromkamp, J., Middelburg, J.J., Soetaert, K., 1995. Production and consumption of biological particles in temperate tidal estuaries. In: Ansell, A.D., Gibson, R.N., Barnes, M. (Eds.), Oceanogr. Mar. Biol. Annu. Rev. University College London Press, London, pp. 1–149.
Henriksen, K., Kemp, W.M., 1988. Nitrification in estuarine and coastal marine sediments. In: Blackburn, T.H., Sørensen, J. (Eds.), Nitrogen Cycling in Coastal Marine Environments. John Wiley & Sons, New York, pp. 207–249.
Hetland, R.D., DiMarco, S.F., 2008. How does the character of oxygen demand control the structure of hypoxia on the Texas-Louisiana continental shelf? Journal of Marine Systems 70, 49–62.
Hooke, R., Jeeves, T.A., 1961. 'Direct search' solution of numerical and statistical problems. Journal of the Association for Computing Machinery (ACM) 8, 212–229.
Imteaz, M.A., Asaeda, T., 2000. Artificial mixing of lake water by bubble plume and effects of bubbling operations on algal bloom. Water Research 34, 1919–1929.
Imteaz, M.A., Asaeda, T., Lockington, D.A., 2003. Modelling the effects of inflow parameters on lake water quality. Environmental Modeling & Assessment 8, 63–70.
Imteaz, M.A., Shanableh, A., Asaeda, T., 2009. Modelling multi-species algal bloom in a lake and inter-algal competitions. Water Science and Technology 60, 2599–2611.
Isleib, R.R., Thuman, A.J., 2011. The Role of estuarine eutrophication models in nutrient criteria development. Proceedings of the Water Environment Federation 2011, 273–298.
Jahnke, R.A., Emerson, S.R., Murray, J.W., 1982. A model of oxygen reduction, denitrification, and organic matter mineralization in marine sediments. Limnology and Oceanography, 610–623.
Jenkins, M.C., Kemp, W.M., 1984. The coupling of nitrification and denitrification in two estuarine sediments. Limnology and Oceanography 29, 609–619.
Jensen, M.H., Lomstein, E., Sorensen, J., 1990. Benthic NH_4^+ and NO_3^- flux following sedimentation of a spring phytoplankton bloom in Aarhus Bight, Denmark. Marine Ecology Progress Series 61, 87–96.
Jiang, M.S., Zhou, M., 2008. Massachusetts Bay Eutrophication Model: 2005 Simulation. Massachusetts Water Resources Authority, p. 82.
Jordan, T.E., Cornwell, J.C., Boynton, W.R., Anderson, J.T., 2008. Changes in phosphorus biogeochemistry along an estuarine salinity gradient: the iron conveyor belt. Limnology and Oceanography 53, 172–184.
Jørgensen, B.B., 1977. Bacterial sulfate reduction within reduced microniches of oxidized marine sediments. Marine Biology 41, 7–17.
Jørgensen, B.B., Revsbech, N.P., 1985. Diffusive boundary layers and the oxygen uptake of sediments and detritus. Limnology and Oceanography 30, 111–122.
Jørgensen, K.S., Sørensen, J., 1988. Two annual maxima of nitrate reduction and denitrification in estuarine sediment (Norsminde Fjord, Denmark). Marine Ecology Progress Series 48, 147–154.
Kana, T.M., Sullivan, M.B., Cornwell, J.C., Groszkowski, K.M., 1998. Denitrification in estuarine sediments determined by membrane inlet mass spectrometry. Limnology and Oceanography 43, 334–339.
Kana, T.M., Cornwell, J.C., Zhong, L., 2006. Determination of denitrification in the Chesapeake Bay from measurements of N_2 accumulation in bottom water. Estuarine Coast 29, 222–231.
Kaplan, I.R., Rittenberg, S.C., 1964. Microbiological fractionation of sulphur isotopes. Journal of General Microbiology 34, 195–212.
Keefe, C.W., 1994. The contribution of inorganic compounds to the particulate organic carbon, nitrogen, and phosphorus in suspended matter and surface sediments of Chesapeake Bay. Estuaries 17, 122–130.
Kelly-Gerreyn, B.A., Trimmer, M., Hydes, D.J., 2001. A diagenetic model discriminating denitrification and dissimilatory nitrate reduction to ammonium in a temperate estuarine sediment. Marine Ecology Progress Series 220, 33–46.
Kemp, W.M., Boynton, W.R., 1992. Benthic-pelagic interactions: nutrient and oxygen dynamics. In: Smith, D., Leffler, M., Mackiernan, G. (Eds.), Oxygen Dynamics in Chesapeake Bay: a Synthesis of Research. Maryland Sea Grant College Park, MD, pp. 149–221.
Kemp, W.M., Sampou, P., Caffrey, J., Mayer, M., Henriksen, K., Boynton, W.R., 1990. Ammonium recycling versus denitrification in Chesapeake Bay sediments. Limnology and Oceanography 35, 1545–1563.
Kemp, W.M., Sampou, P.A., Garber, J., Tuttle, J., Boynton, W.R., 1992. Seasonal depletion of oxygen from bottom waters of Chesapeake Bay: roles of benthic and planktonic respiration and physical exchange processes. Marine Ecology Progress Series 85, 137–152.
Klump, V., Martens, C.S., 1989. The seasonality of nutrient regeneration in an organic-rich coastal sediment: kinetic modeling of changing pore-water nutrient and sulfate distributions. Limnology and Oceanography 34, 559–577.
Krom, M.D., Berner, R.A., 1980. Adsorption of phosphate in anoxic marine sediments. Limnology and Oceanography 25, 797–806.
Krom, M.D., Berner, R.A., 1981. The diagenesis of phosphorus in a nearshore marine sediment. Geochimica et Cosmochimica Acta 45, 207–216.
Lawson, D.S., Hurd, D.C., Pankratz, H.S., 1978. Silica dissolution rates of decomposing phytoplankton assemblages at various temperatures. Journal of American Science 278, 1373–1393.
Lehtoranta, J., Ekholm, P., Pitkänen, H., 2009. Coastal eutrophication thresholds: a matter of sediment microbial processes. Ambio 38, 303–308.
Levins, R., 1966. The strategy of model building in population biology. American Science 54, 421–431.
Lewandoswki, Z., 1982. Temperature dependency of biological denitrification with organic materials addition. Water Research 16, 19–22.
Luff, R., Moll, A., 2004. Seasonal dynamics of the North Sea sediments using a three-dimensional coupled sedimentâ€“ water model system. Continental Shelf Research 24, 1099–1127.
Matisoff, G., Wang, X.S., 1998. Solute transport in sediments by freshwater infaunal bioirrigators. Limnology and Oceanography 43, 1487–1499.
Mayer, L.M., Gloss, S.P., 1980. Buffering of silica and phosphate in a turbid river. Limnology and Oceanography 25, 12–22.
McGlathery, K.J., Sundbäck, K., Anderson, I.C., 2007. Eutrophication in shallow coastal bays and lagoons: the role of plants in the coastal filter. Marine Ecology Progress Series 348, 1–18.
Messer, J.J., Brezonik, P.L., 1984. Laboratory evaluation of kinetic parameters for lake sediment denitrification models. Ecological Modelling 21, 277–286.
Michalopoulos, P., Aller, R.C., 2004. Early diagenesis of biogenic silica in the Amazon delta: alteration, authigenic clay formation, and storage. Geochimica et Cosmochimica Acta 68, 1061–1085.
Miller, D.C., Geider, R.J., MacIntyre, H.L., 1996. Microphytobenthos: the ecological role of the "secret garden" of unvegetated, shallow-water marine habitats. II. Role in sediment stability and shallow-water food webs. Estuaries 19, 202–212.
Nakajima, M., Hayamizu, T., Nishimura, H., 1984. Effect of oxygen concentration on the rates of denitratification and denitrification in the sediments of an eutrophic lake. Water Research 18, 335–338.
Nedwell, D.B., Floodgate, G.D., 1972. Temperature-induced changes in the formation of sulphide in a marine sediment. Marine Biology 14, 18–24.
Otsuki, A., Hanya, T., 1972. Production of dissolved organic matter from dead green algal cells. II. Anaerobic microbial decomposition. Limnology and Oceanography 17, 258–264.
Painter, H.A., Loveless, J.E., 1983. Effect of temperature and pH value on the growth-rate constants of nitrifying bacteria in the activated-sludge process. Water Research 17, 237–248.
Parsons, T.R., Stephens, K., Strickland, J.D.H., 1961. On the chemical composition of eleven species of marine phytoplankters. Journal of the Fisheries Board of Canada 18, 1001–1016.
Pelegrí, S.P., Blackburn, H.T., 1995. Effect of bioturbation by *Neris* sp., *Mya arenaria*, and *Cerastoderma* sp. on nitrification and denitrification in estuarine sediments. Opheila 42, 289–299.
Piña-Ochoa, E., Álvarez-Cobelas, M., 2006. Denitrification in aquatic environments: a cross-system analysis. Biogeochemistry 81, 111–130.
Provoost, P., Braeckman, U., Gansbeke, D.V., Moodley, L., Soetaert, K., Middelburg, J.J., Vanaverbeke, J., 2013. Modelling benthic oxygen consumption and benthic-pelagic coupling at a shallow station in the southern North Sea. Estuarine, Coastal and Shelf Science 120, 1–11.
Rabouille, C., Gaillard, J.F., 1990. The validity of steady-state flux calculations in early diagenesis: a computer simulation of deep-sea silica diagenesis. Deep Sea Research Part A. Oceanographic Research Papers 37, 625–646.
Rabouille, C., Gaillard, J.-F., 1991. Towards the EDGE: early diagenetic global explanation. A model depicting the early diagenesis of organic matter, O_2, NO_3, Mn, and PO_4. Geochimica et Cosmochimica Acta 55, 2511–2525.
Reed, D.C., Slomp, C.P., Gustafsson, B.G., 2011. Sedimentary phosphorus dynamics and the evolution of bottom-water hypoxia: a coupled benthic–pelagic model of a coastal system. Limnology and Oceanography 56, 1075–1092.
Rich, J.J., Dale, O.R., Song, B., Ward, B.B., 2008. Anaerobic ammonium oxidation (Anammox) in Chesapeake Bay sediments. Microbial Ecology 55, 311–320.

Rickert, D., Schlüter, M., Wallmann, K., 2002. Dissolution kinetics of biogenic silica from the water column to the sediments. Geochimica et Cosmochimica Acta 66, 439–455.
Robbins, J.A., Keilty, T., White, D.S., Edgington, D.N., 1989. Relationships among tubificid abundances, sediment composition, and accumulation rates in Lake Erie. Canadian Journal of Fisheries and Aquatic Sciences 46, 223–231.
Roden, E.E., Tuttle, J.H., 1996. Carbon cycling in the mesohaline Chesapeake Bay sediments 2: kinetics of particulate and dissolved organic carbon turnover. Journal of Marine Research 54, 343–383.
Schink, D.R., Fanning, K.A., Pilson, M.E.Q., 1974. Dissolved silica in the upper pore waters of the Atlantic Ocean floor. Journal of Geophysical Research 79, 2243–2250.
Schink, D.R., Guinasso, N.L., Fanning, K.A., 1975. Processes affecting the concentration of silica at the sediment-water interface of the Atlantic Ocean. Journal of Geophysical Research 80, 3013–3031.
Scully, M.E., 2010. The importance of climate variability to wind-driven modulation of hypoxia in Chesapeake Bay. Journal of Physical Oceanography 40, 1435–1440.
Seitzinger, S.P., 1988. Denitrification in freshwater and coastal marine ecosystems: ecological and geochemical significance. Limnology and Oceanography 33, 702–724.
Seitzinger, S., Nixon, S.W., 1985. Eutrophication and the rate of denitrification and N_2O production in coastal marine sediments. Limnology and Oceanography 30, 1332–1339.
Seitzinger, S.P., Nielsen, L.P., Caffrey, J., Christensen, P.B., 1993. Denitrification measurements in aquatic sediments: a comparison of three methods. Biogeochemistry 23, 147–167.
Shieh, W.K., LaMotta, E.J., 1979. The intrinsic kinetics of nitrification in a continuous flow suspended growth reactor. Water Research 13, 1273–1279.
Sigg, L., Stumm, W., 1981. The interaction of anions and weak acids with the hydrous goethite (α-FeOOH) surface. ColSu 2, 101–117.
Slomp, C.P., Malschaert, J.F.P., van Raaphorst, W., 1998. The role of adsorption in sediment-water exchange of phosphate in North Sea continental margin sediments. Limnology and Oceanography 43, 832–846.
Soetaert, K., Middelburg, J.J., 2009. Modeling eutrophication and oligotrophication of shallow-water marine systems: the importance of sediments under stratified and well-mixed conditions. Eutrophication in Coastal Ecosystems, 239–254.
Soetaert, K., Herman, P.M.J., Middelburg, J.J., 1996a. Dynamic response of deep-sea sediments to seasonal variations: a model. Limnology and Oceanography 41, 1651–1668.
Soetaert, K., Herman, P.M.J., Middelburg, J.J., 1996b. A model of early diagenetics processes from the shelf to abyssal depths. Geochimica et Cosmochimica Acta 60, 1019–1040.
Sohma, A., Sekiguchi, Y., Kuwae, T., Nakamura, Y., 2008. A benthic-pelagic coupled ecosystem model to estimate the hypoxic estuary including tidal flat–Model description and validation of seasonal/daily dynamics. Ecological Modelling 215, 10–39.
Spiteri, C., Slomp, C.P., Charette, M.A., Tuncay, K., Meile, C., 2008. Flow and nutrient dynamics in a subterranean estuary (Waquoit Bay, MA, USA): field data and reactive transport modeling. Geochimica et Cosmochimica Acta 72, 3398–3412.
Stenstrom, M.K., Poduska, R.A., 1980. The effect of dissolved oxygen concentration on nitrification. Water Research 14, 643–649.
Stevens, D.K., Berthouex, P.M., Chapman, T.W., 1989. Dynamic model of nitrification in fluidized bed. Journal of Environmental Engineering 115, 910–929.
Stow, C.A., Jolliff, J., McGillicuddy, D.J., Doney, S.C., Allen, J.I., Friedrichs, M.A.M., Rose, K.A., Wallhead, P., 2009. Skill assessment for coupled biological/physical models of marine systems. Journal of Marine Systems 76, 12.
Sundby, B., Gobeil, C., Silverberg, N., Mucci, A., 1992. The phosphorus cycle in coastal marine sediments. Limnology and Oceanography 37, 1129–1145.
Testa, J.M., Kemp, W.M., 2012. Hypoxia-induced shifts in nitrogen and phosphorus cycling in Chesapeake Bay. Limnology and Oceanography 57, 835–850.
Tromp, T.K., Van Cappellen, P., Key, R.M., 1995. A global model for the early diagenesis of organic carbon and organic phosphorus in marine sediments. Geochimica et Cosmochimica Acta 59, 1259–1284.
Turekian, K.K., Benoit, G.J., Benninger, L.K., 1980. The mean residence time of plankton-derived carbon in a Long Island Sound sediment core: a correction. Estuarine and Coastal Marine Science 11, 583.
Ullman, W.J., Aller, R.C., 1989. Nutrient release rates from the sediments of Saginaw Bay, Lake Huron. Hydrobiologia 171, 127–140.
Upchruch, J.B., Edzwald, J.K., O'Melia, C.R., 1974. Phosphates in sediments of Pamlico estuary. Environmental Science and Technology 8, 56–58.
Van Cappellen, P., Berner, R.A., 1988. A mathematical model for the early diagenesis of phosphorus and fluorine in marine sediments; apatite precipitation. Journal of American Science 288, 289–333.
Van Cappellen, P., Linqing, Q., 1997a. Biogenic silica dissolution in sediments of the Southern Ocean. I. Solubility. Deep Sea Research 44, 1109–1128.
Van Cappellen, P., Linqing, Q., 1997b. Biogenic silica dissolution in sediments of the Southern Ocean. II. Kinetics. Deep Sea Research 44, 1129–1149.
Vanderborght, J.-P., Wollast, R., Billen, G., 1977a. Kinetic-models of diagenesis in disturbed sediments. Part 1. Mass-transfer properties and silica diagenesis. Limnology and Oceanography 22, 787–793.
Vanderborght, J.-P., Wollast, R., Billen, G., 1977b. Kinetic-models of diagenesis in disturbed sediments. Part 2. Nitrogen diagenesis. Limnology and Oceanography 22, 787–793.
Vosjan, J.H., 1974. Sulphate in water and sediment of the Dutch Wadden Sea. Netherlands Journal of Sea Research 8.
Wang, Y., Van Cappellen, P., 1996. A multicomponent reactive transport model of early diagenesis: application to redox cycling in coastal marine sediments. Geochimica et Cosmochimica Acta 60, 2993–3014.
Wang, H., Appan, A., Gulliver, J.S., 2003. Modeling of phosphorus dynamics in aquatic sediments: II - examination of model performance. Water Research 37, 3939–3953.
Warwick, J.J., 1986. Diel variation of in-stream nitrification. Water Research 20, 1325–1332.
Westrich, J.T., Berner, R.A., 1984. The role of sedimentary organic matter in bacterial sulfate reduction: the G Model tested. Limnology and Oceanography 29, 236–249.
Westrich, J.T., Berner, R.A., 1988. The effect of temperature on rates of sulfate reduction in marine sediments. Geomicrobiology Journal 6, 99–117.
Wheatland, A.B., 1954. Factors affecting the formation and oxidation of sulphides in a polluted estuary. Journal of Hygiene (London) 52, 194–210.
Wong, G.T.F., Grosch, C.E., 1978. A mathematical model for the distribution of dissolved silicon in interstitial waters - an analytical approach. Journal of Marine Research 36, 735–750.
Yamada, S.S., D'Elia, C.F., 1984. Silicic acid regeneration from estuarine sediment cores. Marine Ecology Progress Series. 18, 113–118.
Young, J.C., Thompson, L.O., Curtis, D.R., 1979. Control strategy for biological nitrification systems. Journal (Water Pollution Control Federation), 1824–1840.